Ore Geology Reviews 149 (2022) 105068

Contents lists available at ScienceDirect

Ore Geology Reviews

journal homepage: www.elsevier.com/locate/oregeorev

The trace element chemistry of quartz in carbonatite-related REE deposits: Implication for REE exploration

Wei Zhang [a,b], Wei Terry Chen [b,c,*], Xing-Chun Zhang [b], Yan-Wen Tang [b]

[a] School of Earth Sciences, Yunnan University, Kunming 650500, China
[b] State Key Laboratory of Ore Deposit Geochemistry, Institute of Geochemistry Chinese Academy of Sciences, Guiyang 550081, China
[c] University of Chinese Academy of Sciences, Beijing 10039, China

ARTICLE INFO

Keywords:
Quartz
Trace elements
Carbonatite-related REE deposit
Exploration

ABSTRACT

Quartz is a common gangue mineral in many magmatic-hydrothermal ore deposits (e.g., porphyry, epithermal and skarn deposits) and its trace element composition was widely used to constrain ore genesis. Quartz is also a common phase in carbonatite-related rare earth element (REE) deposits, but its geochemical characteristics and significance for ore genesis have not previously been documented in this environment. In this contribution, we report in-situ LA-ICP-MS trace element compositions of quartz from seven carbonatite-related REE deposits, namely the Maoniuping, Lizhuang and Dalucao deposits in the Mianning-Dechang REE metallogenic belt, SW China and the Miaoya, Taipingzhen, Huangshuian and Huanglongpu deposits in the Qinling REE metallogenic belt, Central China. Rare earth element mineralization in these deposits is associated with well-developed hydrothermal systems in which the dominant REE minerals, bastnäsite, parisite, and monazite, are intergrown with aegirine-augite, arfvedsonite, calcite, fluorite, barite, and quartz. The results show that quartz grains from the carbonatite-related REE deposits are characterized by low budgets of trace elements, of which Al is generally less than 50 ppm whereas others are generally less than 10 ppm. In general, the trace element concentrations in quartz from different deposits are similar (the total concentration is commonly <50 ppm), and are distinguishable from those of quartz in other magmatic-hydrothermal systems. The low concentration of trace elements in carbonatite-related REE deposits is controlled by the unusual nature of carbonatitic magmas and their derived fluids, and thus can be used for defining the affinity of hydrothermal REE systems that are of unknown origin. Significantly, the trace element chemistry of quartz samples collected from a cross-section in the open pit of the Maoniuping REE deposit displays a systematic spatial variation such that the concentrations of Al, Ti, Na, and K decrease with increasing distance of the samples from carbonatites. This spatial variation correlates well with the variation of physio-chemical conditions during the evolution of ore-forming fluids. This implies that the geochemistry of quartz can be used as a vector detecting the concealed carbonatite intrusions in carbonatite-related REE deposits.

1. Introduction

Quartz is one of the most important and abundant gangue minerals in many magmatic-hydrothermal ore deposits. It forms over a wide range of temperatures and pressures from fluids of diverse origins and compositions, and its trace element composition has been shown to be sensitive to physicochemical conditions in the environment of deposition (Landtwing and Pettke, 2005; Götze, 2009; Rusk, 2012; Breiter et al., 2013; Monnier et al., 2018). Consequently, the chemistry of quartz has been used to constrain ore genesis in a variety of magmatic-hydrothermal deposits, e.g., porphyry Cu (Mo-Au) (Müller et al., 2010; Maydagán et al., 2015; Mao et al., 2017; Rottier and Casanova, 2020), skarn Cu (Au) (Zhang et al., 2019b), epithermal Cu (Au-Ag) and Sb (Rusk et al., 2011; Tanner et al., 2013; Monnier et al., 2021), Carlin-type Au (Li et al., 2020; Yan et al., 2020), and greisen related sn-W deposits (Breiter et al., 2017; Monnier et al., 2018; Launay et al., 2021). To our knowledge, however, no studies have been published on the chemistry of quartz in carbonatite-related magmatic-hydrothermal REE deposits, even though quartz is a common phase in such systems. Although mineralizing fluids exsolved from carbonatitic magmas have been shown to be very different from those in other magmatic-hydrothermal systems related to silicate magmas (Bühn and Rankin,

* Corresponding author at: State Key Laboratory of Ore Deposit Geochemistry, Institute of Geochemistry Chinese Academy of Sciences, Guiyang 550081, China
E-mail address: chenwei@mail.gyig.ac.cn (W. Terry Chen).

https://doi.org/10.1016/j.oregeorev.2022.105068
Received 7 June 2022; Received in revised form 31 July 2022; Accepted 17 August 2022
Available online 22 August 2022

1999; Williams-Jones and Palmer, 2002; Rankin, 2005; Xie et al., 2015; Walter et al., 2021), it is still unclear if quartz in the carbonatite-related REE deposits has distinctive trace element characteristics that enable its use as an indicator for exploring REE mineralization.

In this contribution, we conduct combined mineralogical and LA-ICP-MS trace element analyses of quartz from seven carbonatite-related REE deposits in the Mianning-Dechang and Qinling REE belts, two well-known REE metallogenic belts in China. Our study reports the first in-situ trace element compositions of quartz from carbonatite-related REE deposits, and shows that quartz from these deposits has geochemical characteristics distinguishable from those in other types of magmatic-hydrothermal systems. In addition, systematic analyses of quartz samples in a cross-section of the Maoniuping REE deposit reveal that the trace element composition of quartz varies systematically with distance from the causative carbonatites. These findings suggest that the chemistry of quartz is able to fingerprint the nature and evolution of ore-forming fluids and can be used to improve the efficiency of REE exploration.

2. Geological background

2.1. Mianning-Dechang REE metallogenic belt

The Mianning-Dechang REE metallogenic belt, located at the western margin of the Yangtze Block in South China, is bounded by the NS-striking Yalongjiang and Anninghe faults (Fig. 1a). The basement in the belt consists predominantly of Archean amphogneiss and granulite and Proterozoic metadolomite, covered by Paleozoic-Mesozoic clastic,

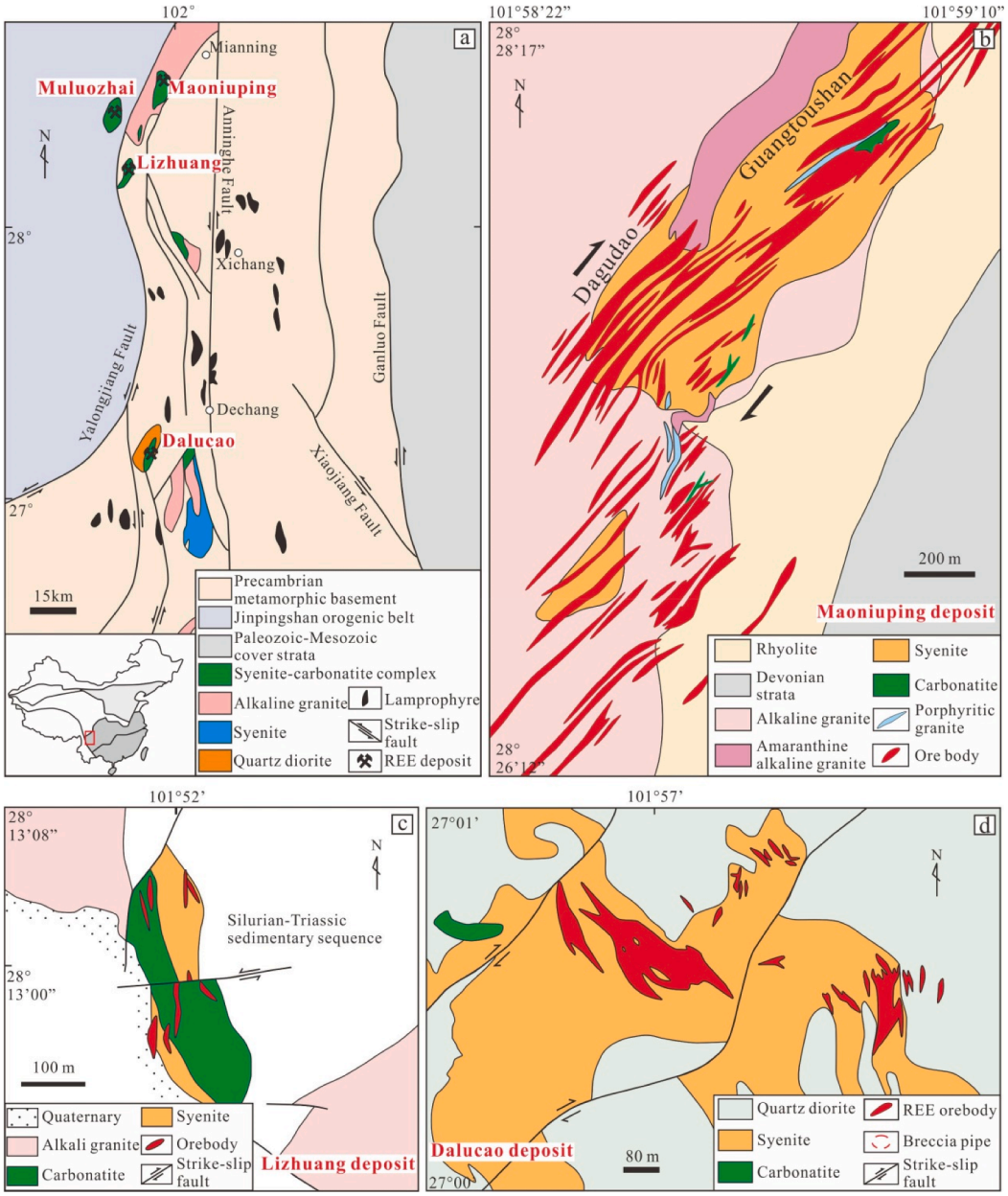

Fig. 1. (a) Sketch tectonic map of the Mianning-Decang REE metallogenic belt. Also shown are the locations of carbonatite-related REE deposits (modified from Yuan et al., 1995). (b) Geological map of the Maoniuping REE deposit showing the relationships among REE orebodies, carbonatite, syenite, alkaline granite, and alkaline granite (modified from Hou et al., 2009). (c) Geological map of the Lizhuang REE deposit showing the distribution of carbonatite and associated REE orebodies (modified from Hou et al., 2009). (d) Geological map of the Dalucao REE deposit showing the relationships among breccia orebodies, carbonatites, syenite and quartz diorite (modified from Hou et al., 2009).

carbonate, and volcanic sequences (Cong, 1988; Luo et al., 1998). A series of Cenozoic strike-slip faults, which were developed to accommodate the stress and strain of the 65–50 Ma Indo-Asian collision from the west (Fig. 1a), served as conduits for subsequent mantle-derived magmas that were responsible for the formation of lamprophyres and carbonatites (Hou et al., 2006, 2009).

The Mianning-Dechang belt hosts a number of REE deposits with more than 4 Mt of total REO resources (Hou et al., 2009; Xie et al., 2016). Examples include the Maoniuping (25 Ma), Muluozhai (27 Ma) and Lizhuang (28 Ma) deposits in the north and the Dalucao deposit (12 Ma) in the south (Fig. 1a). These REE deposits are all spatially associated with coeval carbonatite-syenite complexes, although the REE mineralization is interpreted to be genetically related to the carbonatites (Hou et al., 2009; Xie et al., 2009, Xie et al., 2015). The geology and mineralization styles of a selection of these deposits are described below and summarized in Table 1.

2.1.1. *Maoniuping deposit*

The Maoniuping deposit, containing a total REO reserve of 3.17 Mt at an average grade of 2.95 wt% (Geology Exploration Team No. 109), is

Table 1
Geological characteristics of representative carbonatite-related REE deposits in the Mianning-Dechang and Qinling REE belts.

Deposit	Tonnages and Grades	Host rock	Wall rocks	Ore type	Mineral assembly of ores	alternation	Age	References
Mianning-Dechang REE belt								
Maoniuping	3.17 Mt @ 2.95 % REO	Syenite-carbonatite complex	Granite, rhyolite	Pegmatitic, breccia, disseminated, hydrothermal veins and stockwork	Aegirine-augite + arfvedonite + calcite + quartz + fluorite + barite + celestite + biotite + K-feldspar + fluorphlogopite + bastnäsite	Fenitization, carbonatization, argillization	Zircon U-Pb age: 26.6 ± 0.3 Ma; Bastnaesite U-Th-Pb age: 25.7 ± 0.2 Ma	Hou et al., 2009;Xie et al., 2015; Ling et al., 2016; Liu et al., 2018
Lizhuang	5764 t @1.5 % REO	Syenite-carbonatite complex	Granite, Silurian-Triassic sedimentray rocks	Banded, disseminated, hydrothermal veins and stockwork	Aegirine-augite + arfvedonite + calcite + quartz + fluorite + barite + celestite + biotite + fluorphlogopite + bastnäsite	Fenitization, carbonatization	Zircon U-Pb age: 28.8 ± 0.3 Ma; Bastnaesite U-Th-Pb age: 28.4 ± 0.2 Ma	Hou et al., 2009;Xie et al., 2015; Ling et al., 2018
Dalucao	0.76 Mt @ 5.21 % REO	Syenite-carbonatite complex	Quarts diorite	Breccia, massive, disseminated, hydrothermal veins and stockwork	Aegirine-augite + arfvedonite + calcite + quartz + fluorite + barite + celestite + biotite + K-feldspar + bastnäsite	Fenitization, carbonatization, argillization	Zircon U-Pb age: 12.7 ± 0.2 Ma; Bastnaesite U-Th-Pb age: 11.9 ± 0.2 Ma	Hou et al., 2009; Liu et al., 2015; Ling et al., 2017
Qinling REE belt								
Miaoya	1.21 Mt @ 1.5 % REO; 0.93 Mt @ 0.1 wt% Nb_2O_5	Syenite-carbonatite complex	Meta-quartz keratophyre of Yaolinghe Group, schist of Meiziya Group	Mineralized part of syenite-carbonatite complex (dissminated), hydrothermal veins and stockwork	Syenite: K-feldspar + albite + biotite + quartz + zircon + apatite + monazite + columbite; Carbonatite: calcite + K-feldspar + biotite + apatite + monazite + columbite + bastnäsite + pyrochlore + quartz + pyrite + magmatite	Carbonatization, sericitization	Zircon U-Pb age: 443 ± 4 Ma and 426 ± 8 Ma; Monazite U-Th-Pb age: 414 ± 11 Ma and ~ 230 Ma; Bastnaesite U-Th-Pb age: 206 ± 4 Ma;	Xu et al., 2014; Zhu et al., 2016; Ying et al., 2017;Zhang et al., 2019a
Taipingzhen	0.15 Mt @ 2.32 % REO	Carbonatite	volcanic rocks, Amphibolite schist of Erlangping Group	Massive, disseminated, hydrothermal veins and veinlets	Quartz + fluorite + barite + celestite + calcite + apatite + k-feldspar + albite + biotite + pyrite + magnetite + bastnäsite + parasite + monazite + molybdenite + chalcopyrite	K-Na alteration, silicification, sericitization	Bastnaesite U-Th-Pb age: 425.6 ± 4.8 Ma, 415.8 ± 7.3 Ma	Li et al., 2017;Zhang et al., 2019a
Huangshuian	0.4 Mt Mo @ 0.06 % Mo; REE is not aviliable	Carbonatite	High-grade Metamorphic rocks (gneiss) of Taihua Group	Disseminated, hydrothermal veins and veinlets	Calcite + quartz + barite + celestite + fluorite + K-feldspar + apatite + pyrite + galena + molybdenite + bastnäsite	Silicification, K-feldspathization, pyritization	Bastnaesite U-Th-Pb age: 206.5 ± 3.8 Ma; Molybdenite re-Os age: 209.5 ± 4.2 Ma	Huang et al., 2009; Li et al., 2014; Zhang et al., 2019a
Huanglongpu	0.25 Mt @ 0.07 % Mo; REE is not available	Carbonatite	High-grade Metamorphic rocks (gneiss) of Taihua Group	Disseminated, hydrothermal veins and veinlets	Calcite + quartz + barite + celestite + fluorite + K-feldspar + apatite + pyrite + galena + molybdenite + bastnäsite	Silicification, K-feldspathization, pyritization	Monazite U-Th-Pb age: 213.6 ± 4.0 Ma; Molybdenite re-Os age: 221.5 ± 0.3 Ma	Stein et al., 1997; Huang et al., 2009; Song et al., 2016

the largest REE deposit in the Mianning-Dechang belt (Hou et al., 2009; Xie et al., 2016). Carbonatites in the deposit are present in the mine area as plugs and dikes intruding the syenites (Fig. 1b). The plugs are outcropped in the Guangtoushan area with an exposed area of 150 m^2, while the dikes are generally 0.2 to 2 m in width and present at the bottom of the orebodies in the Dagudao area (Fig. 2a). The carbonatites have similar composition dominantly of calcite (50–90 % by volume) with subordinate aegirine-augite, arfvedsonite, barite, quartz and fluorite (Fig. 3a–b). About 71 orebodies with length of 10 to 1168 m and thickness of 1.2 to 32 m have been identified. These orebodies are lenses and banded in shape and dip steeply towards NW at 65–80° (Fig. 1b). REE mineralization occurs mainly as veinlets, stringers and stockworks crosscutting the syenites and older granites and rhyolites, and is associated with extensive fenitization (Hou et al., 2009; Liu et al., 2019). Fenitization is manifested as secondary aegirine-augite, arfvedsonite and associated Mg-rich biotite and its intensity is gradually decreased with increase of distance from the carbonatites.

Mineralization in the Maoniuping deposit is unevenly distributed, and thus the orebodies are generally divided into bottom, middle and top units (Fig. 2b). The bottom unit, which is close to the underlying carbonatites and hosts the most extensive fenitization (Fig. 3c), comprises 1 to 30 cm wide veins and stockworks with a mineral assemblage of aegirine-augite, arfvedsonite, fluorphlogopite and minor quartz, K-feldspar, biotite, calcite, and bastnäsite. The middle unit is characterized by relatively weak fenitization but extensive REE mineralization compared to the bottom unit, corresponding to relatively low contents of aegirine-augite and arfvedsonite and high contents of fluorite, barite, quartz, and bastnäsite (Fig. 3d–e). The top unit has the weakest fenitization and undergone argillization in which calcite and barite grains are variably weathered and leached. The veins in this unit are 5 to 50 cm in thickness and consist mainly of fluorite, quartz, barite, calcite, and bastnäsite with minor aegirine-augite, arfvedsonite, biotite, and fluorphlogopite (Fig. 3f).

2.1.2. Lizhuang deposit

The Lizhuang deposit, 20 km south of the Maoniuping deposit, is a small REE deposit with a total REO reserve of 5764 t at an average REO grade of 1.5 wt% (Xie et al., 2016). The carbonatites are present as sills and dikes (Fig. 1c) and consist mainly of calcite (50–80 % by volume) and subordinate aegirine-augite, fluorite, quartz and barite. This deposit consists of a number of small lenses that are ~ 30 to 100 m length and 2.2 to 11.6 m thick. The REE mineralization occurs as banded and vein-type (or stockwork) ores and is associated with extensive fenitization that crystallized variable proportions of secondary aegirine-augite, arfvedsonite and phlogopite. Banded ores, occurring mostly in the contact zone between the carbonatite and wall rocks, have a mineral assemblage of calcite, barite, fluorite, bastnäsite, and minor biotite and quartz. The vein-type ores, characterized by 0.5–3 cm wide veins, consist mainly of calcite, fluorite, quartz, barite, aegirine-augite with minor pyrite, pyrrhotite, bastnäsite and monazite (Fig. 3g).

2.1.3. Dalucao deposit

The Dalucao deposit, containing a total reserve of 0.76 Mt REO at an average grade of 5 wt% (Hou et al., 2009), is the second largest REE deposit in the Mianning-Dechang belt. Carbonatites are present as dikes (0.5–2 m in width) intruding the syenite and quartz diorite (Fig. 1d). They are composed mainly of calcite (70 % by volume) with minor proportions of aegirine–augite, biotite, barite, and quartz. The REE ore is mainly breccia-type that composed of angular to rounded syenite and carbonatite clast cemented by a hydrothermal matrix. The hydrothermal matrix is composed of calcite, quartz, fluorite, barite, and bastnäsite with minor aegirine-augite and arfvedsonite. There are also minor vein-type ores, in which the veins are 1 to 30 cm in width and are composed of variable proportions of barite, quartz, fluorite, fluorite, aegirine-augite, and bastnäsite (Fig. 3h). Fenitization is the dominant alteration surrounding the carbonatites and orebodies, but its intensity is relatively weak compared to that of the Maoniuping and Lizhuang deposits. At the edge of the orebodies, the fenitization is overprinted by carbonatization which has an assemblage of calcite, quartz, fluorite, barite, celestine and minor pyrite and bastnäsite.

2.2. Qinling REE metallogenic belt

The Qinling Orogenic belt comprises four tectonic units, namely the Southern North China Craton, North Qinling, South Qinling, and Northern Yangtze Block from north to south (Fig. 4a). Numerous carbonatite-related REE deposits have been discovered in this orogenic belt in recent years, and collectively form the Qinling REE metallogenic belt (Zhang et al., 2019a). Some examples of deposits in the belt are the 440–430 Ma Miaoya and Shaxiongdong REE-Nb deposits in South Qinling, the 410 Ma Taipingzhen REE deposit in North Qinling and the 220–210 Ma Huayangchuan U-Nb-REE, Huanglongpu and Huangshuian Mo-Pb-REE deposits in Southern North China Craton. The available data suggests that the REE belt contains an estimated total of approximately 2

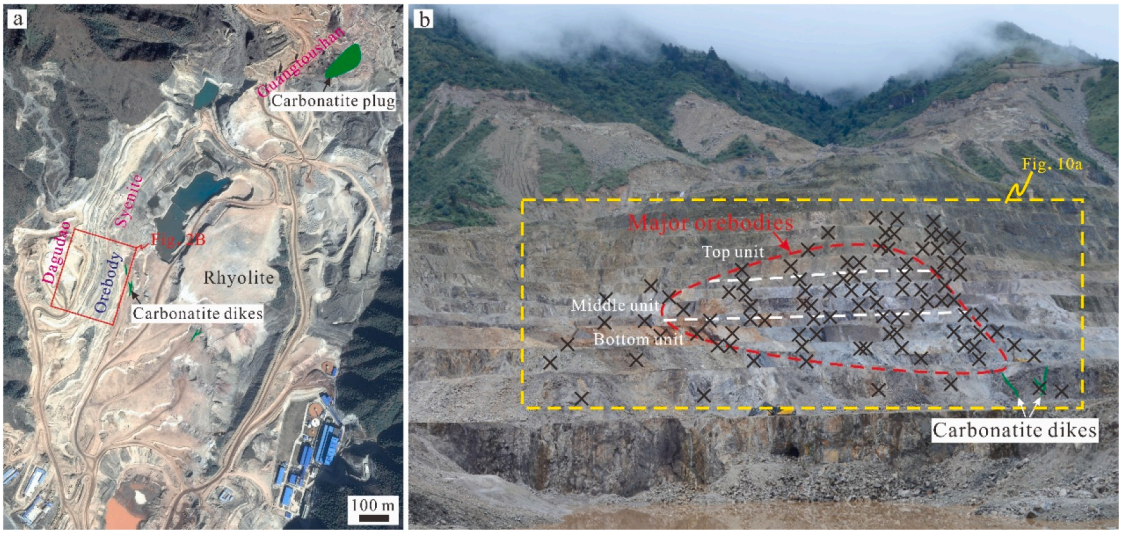

Fig. 2. Geological features of the Maoniuping REE deposit. (a) An overview of the open pit mine (from Google Map), showing the location of carbonatites, syenite, rhyolite, and major orebodies. (b) The western section of the open pit mine, showing the bottom, middle and top units of the orebody, and locations of carbonatite dikes and quartz samples.

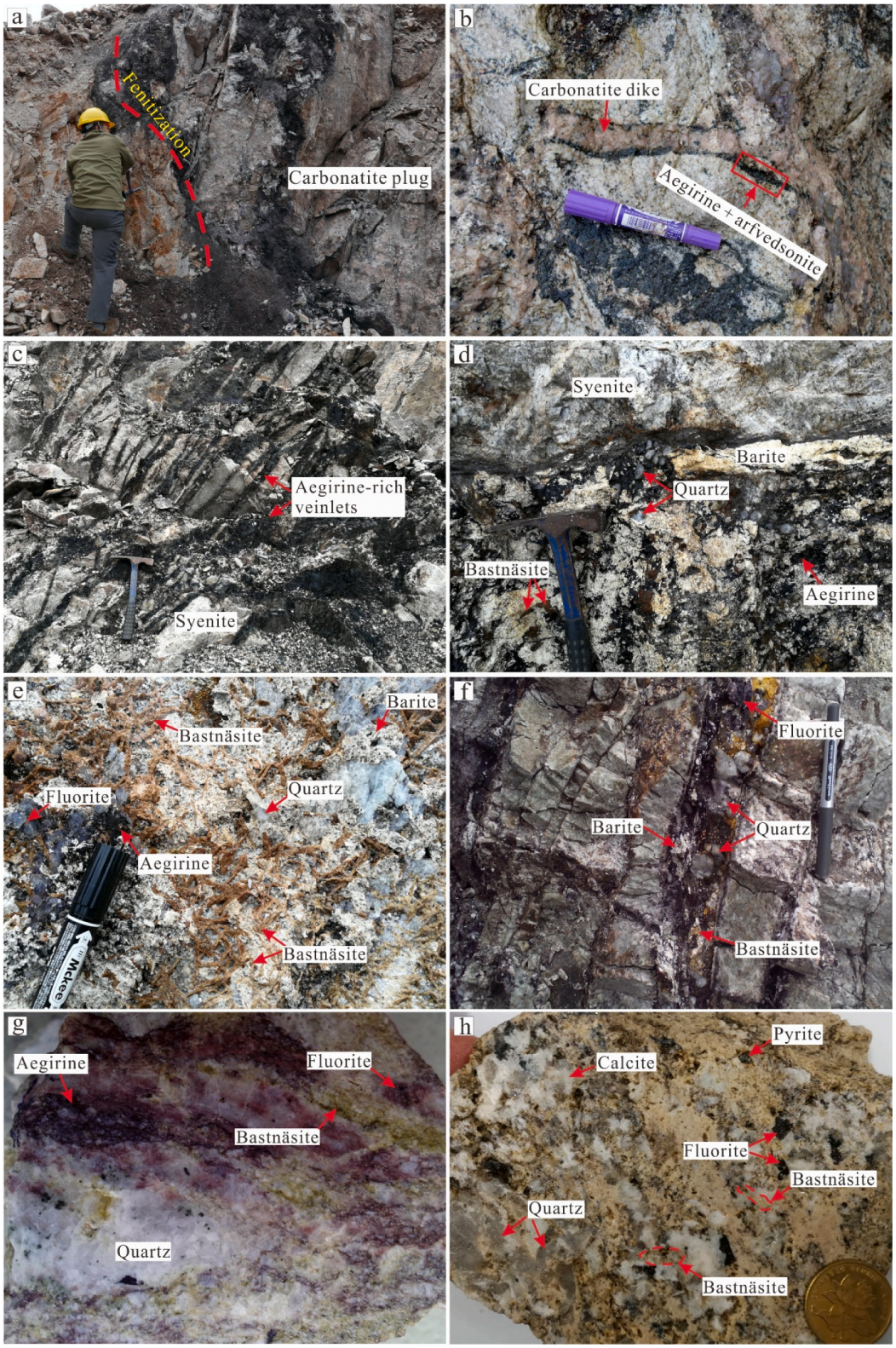

Fig. 3. Photomacrographs of various ores in the carbonatite-related REE deposits of the Mianning-Decang belt. (a) Carbonatite plug with intensive fenitization in the northeast of the Maoniuping deposit. (b) Thin carbonatite dike intrude syenite with intensive fenitization at the bottom of major orebodies in the Maoniuping deposit. (c) Aegirine-augite-rich veins/veinlets in the bottom unit of the Maoniuping deposit. Note that the vein/veinlets are 1 to 30 cm in width. (d) A thick vein in the middle unit of the Maoniuping deposit, containing coarse-grained aegirine-augite, fluorite, barite, quartz, calcite, and bastnäsite. (e) High-grade ore in the middle unit of the Maoniuping deposit, consisting of egirine-augite, barite, fluorite, quartz and abundant bastnäsite (greater than 30 vol%). (f) Intergrowth of quartz with fluorite, barite, calcite, and bastnäsite in a thick vein in the top unit of the Maoniuping deposit. (g) Intergrowth of quartz, fluorite, and bastnäsite in the Lizhuang deposit. (h) Vein-type ore in the Dalucao deposit, consisting of calcite, quartz, fluorite, barite, and bastnäsite.

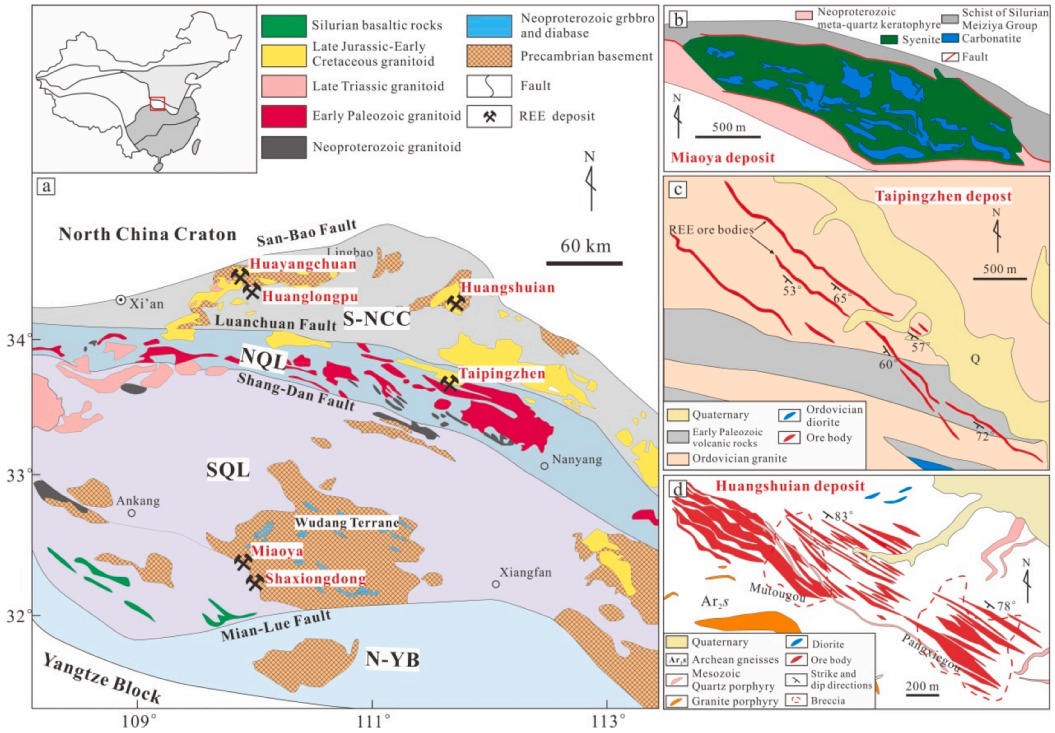

Fig. 4. (a) Tectonic sketch of the Qinling Orogenic Belt. Also shown are locations of carbonatite-related REE deposits. (b) Simplified geological map of the Miaoya REE-Nb deposit that is characterized by mineralized carbonatite and syenites (modified from Xu et al., 2014). (c) Simplified geological map of the Taipingzhen REE deposit showing the location of REE orebodies (modified from Li et al., 2017). (d) Simplified geological map of the Huangshuian Mo-(REE) deposit showing the distribution of carbonatite-related orebodies (modified from Cao et al., 2014). Abbreviations: S-NCC = Southern North China Craton, NQL = North Qinling unit, SQL = South Qinling unit, *N*-YB = Northern Yangtze Block.

Mt REO resources (Qian and Li, 1996; Li et al., 2017; Gao et al., 2017; Zhang et al., 2019a). Detailed descriptions of these deposits are provided in studies by Xu et al. (2010, 2014), Cao et al. (2014), Song et al. (2015, 2016), Li et al. (2017), Ying et al. (2017), Smith et al. (2018), Zhang et al. (2019a) and Zheng et al. (2020), and are briefly summarized below.

2.2.1. *Miaoya REE-Nb deposit*

The Miaoya REE-Nb deposit, containing an estimated reserve of 1.21 Mt REO at an average grade of 1.5 wt% (Qian and Li, 1996), is the largest REE deposit in the Qinling REE metallogenic belt. It is a REE-Nb mineralized syenite-carbonatite complex, which covers an area of 6.5 km^2 and intrudes the metamorphic rocks of the Yaolinghe and Meiziya Group (Fig. 4b). Syenite, the dominant phase of the complex, is composed mainly of K-feldspar, plagioclase, microcline with minor amounts of albite, biotite, sericite, calcite, apatite and monazite. Carbonatites, which are present as stocks and/or dikes intruding the syenites, are dominated by medium- to fine-grained calcite (80 % by volume) with variable K-feldspar, quartz, biotite, fluorapatite, monazite, columbite, bastnäsite, ilmenite, and magnetite. The REE ores are essentially REE-Nb-mineralized (economic) syenites and carbonatites in the complex, associated with numerous hydrothermal veins of variable thickness (0.1 to 10 cm) composed of calcite, ankerite, fluorite, quartz, pyrite, monazite, albite, biotite, fluorapatite, and bastnäsite (Fig. 5a).

2.2.2. *Taipingzhen REE deposit*

The Taipingzhen REE deposit contains an estimated reserve of 0.15 Mt REO with an average grade of 2.32 wt% (Li et al., 2017). Carbonatites are present as dikes (0.5 to 2 m in width) intruding the foliated Zhangjiazhuang plagiogranite. They are composed mainly of calcite (~70 % by volume) and variable proportions of quartz, biotite, barite, pyrite, magnetite and bastnäsite. The orebodies take the form of sheets hosted in the Erlangping Group and Zhangjiazhuang plagiogranite and structurally controlled by subparallel NWW-trending faults and shear zones (Fig. 4c). The mineralization is commonly of vein or veinlets-type. The REE-rich veins have widths ranging from several centimeters to few meters and generally dip to the northwest (Fig. 5b). This deposit is characterized by containing a variety of REE minerals including fluocerite, bastnäesite, parisite, synchysite, monazite, taipingite, törnebohmite, and gatelite (Zhang et al., 2019a; Qu et al., 2019a, 2019b, 2020).

2.2.3. *Huanglongpu and Huangshuian Mo-REE deposits*

The Huanglongpu and Huangshuian deposits in the Southern North China Craton are similar in terms of mineralization styles. The two deposits host important Mo resources of 0.25 (average grade of 0.071 wt%) and 0.4 (average grade of 0.062 wt%) Mt, respectively, and the REEs are by-product metals (Xu et al., 2010; Kynicky et al., 2012; Zhang et al., 2021). The carbonatites in both deposits are present as plugs and dikes intruding the metamorphic rocks of the Archean Taihua Group (Fig. 4d). They are generally pink in color and are composed dominantly of calcite, quartz, barite, and fluorite with subordinate K-feldspar, biotite, apatite, pyrite, and magnetite (Fig. 5c). The REE and Mo mineralization are closely associated, and are concentrated in veins or stockworks cross-cutting the carbonatites and/or metamorphic rocks of the Taihua Group (Fig. 5d). The veins or stockworks are 0.1–5 cm in width and are composed mainly of quartz, barite, celestite, fluorite, apatite and calcite with minor sulfides (pyrite, molybdenite, galena, sphalerite and chalcopyrite) and REE minerals (bastnäsite, parisite, and monazite).

3. Sampling and analytical methods

3.1. *Sampling*

Quartz from the Maoniuping, Lizhuang and Dalucao deposits in the Mianning-Dechang belt and the Miaoya, Taipingzhen, Huanglongpu and

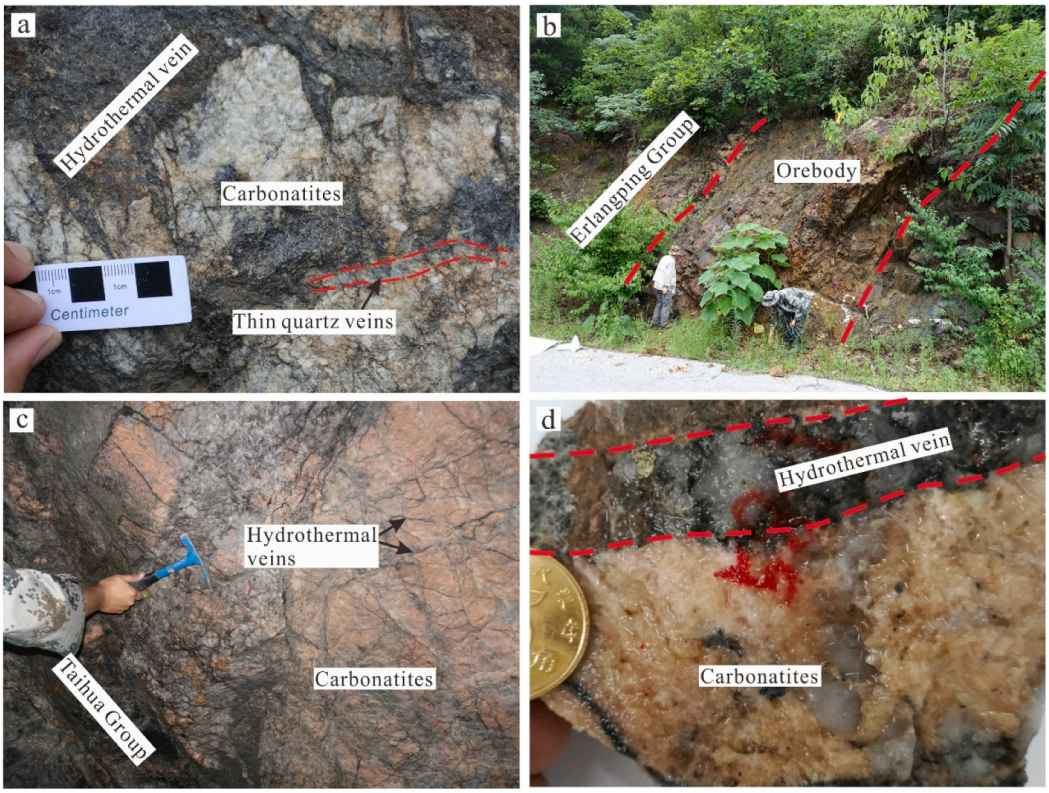

Fig. 5. Photomacrographs of various ores/wall rocks in the carbonatite-related REE deposits of the Qinling belt. (a) Thick calcite-barite-fluorite-quartz vein and thin quartz veinlet distributing in the carbonatites of the Miaoya deposit. (b) Orebody present as sheets intersecting the amphibolite of the Erlangping Group in the Taipingzhen deposit. (c) Carbonatite plug intruding the metamorphic rocks of Taihua Group in the Huangshuian deposit. (d) Quartz-pyrite veins crosscutting carbonatites in the Huangshuian deposit.

Huangshuian deposits in the Qinling belt was selected for trace element analyses. All the quartz samples were collected from typical hydrothermal REE ores in which the quartz is intergrown with variable amounts of aegirine, aegirine-augite, arfvedsonite, fluorite, barite, celestite and REE minerals (e.g., bastnäsite, monazite). In order to understanding spatial variations of quartz chemistry within an individual deposit, detailed sampling of quartz was also conducted on a cross-section in the open pit mine of the Maoniuping REE deposit (Fig. 2b). It is notable that the selected cross-section contains the bottom, middle and top units of orebodies described above (Fig. 2b).

3.2. Backscatter electron (BSE) and cathodoluminescence (CL) analyses

Backscatter electron (BSE) and cathodoluminescence (CL) images were taken of polished thin sections using a JSM-7800F type thermal field-emission scanning electron microscope (SEM) equipped with a TEAM Apollo XL energy dispersive spectrometer and a Mono CL4 cathodoluminescence spectrometer from Gatan at the State Key Laboratory of Ore Deposit Geochemistry (SKLODG), Institute of Geochemistry, Chinese Academy of Sciences, Guiyang, China. The polished thin sections were carbon-coated to avoid electrical charge build up during operation. The instrument was operated at an acceleration voltage of 15 kV and a probe current of ~ 10nA. The minimum magnification of the detector was 120 × when obtaining CL images of the quartz.

3.3. In-situ LA-ICP-MS trace elemental analysis

In-situ trace element analyses of quartz were performed at SKLODG using an Agilent 7900 ICP-MS equipped with a GeoLasPro 193 nm ArF excimer laser. Details of the analytical procedures and instrumental operating conditions are provided by Lan et al. (2017). A laser energy density of 10 J/cm^2, a repetition rate of 10 Hz, and a spot size of 44 μm were used during the analyses. The laser ablation aerosol was transferred from the ablation cell to the ICP-MS by helium, which was mixed with argon before entering the torch. Each spot analysis consisted of an approximate 20 s background acquisition and 50 s sample data acquisition. A total of 21 trace elements including ^{7}Li, ^{9}Be, ^{11}B, ^{23}Na, ^{24}Mg, ^{27}Al, ^{31}P, ^{39}K, ^{49}Ti, ^{55}Mn, ^{56}Fe, ^{71}Ga, ^{74}Ge, ^{75}As, ^{85}Rb, ^{88}Sr, ^{111}Cd, ^{118}Sn, ^{121}Sb and ^{137}Ba were analyzed. The National Institute of Standards and Technology reference (NIST) material SRM 610 and SRM 612 were used as external standards (Pearce et al., 1997). A natural quartz standard from Shandong province, China, was used as a second standard to ensure accurate results (Audétat et al., 2015). Each standard sample was measured twice after 10 analyses of unknown quartz. Off-line data selection and integration were performed by ICPMSDataCal (Liu et al., 2008) using Si as the internal standard. Before analyses, the target spots were carefully selected on the basis of transmitted light, BSE and CL images to avoid fluid and mineral inclusions. In addition, accidental ablation of inclusions during analyses was also carefully monitored through the time-resolved analytical signals.

4. Results

4.1. Mineralogy of quartz

Quartz is a major phase in the orebodies from all the carbonatite-related REE deposits (Fig. 6). It is present as subhedral to euhedral crystals with a variety of diameter from several millimeters to several centimeters. It contains abundant mineral inclusions including aegirine-augite, arfvedsonite, barite fluorite, calcite, apatite and bastnäsite (Fig. 6a, 6h, 6i). Fluid inclusions in the quartz include high-density, CO_2-rich inclusions, solid-bearing brine inclusions, and aqueous liquid inclusions (Fig. 6c). Quartz grains from all the carbonatite-related REE deposits exhibit either homogeneous texture or euhedral oscillatory

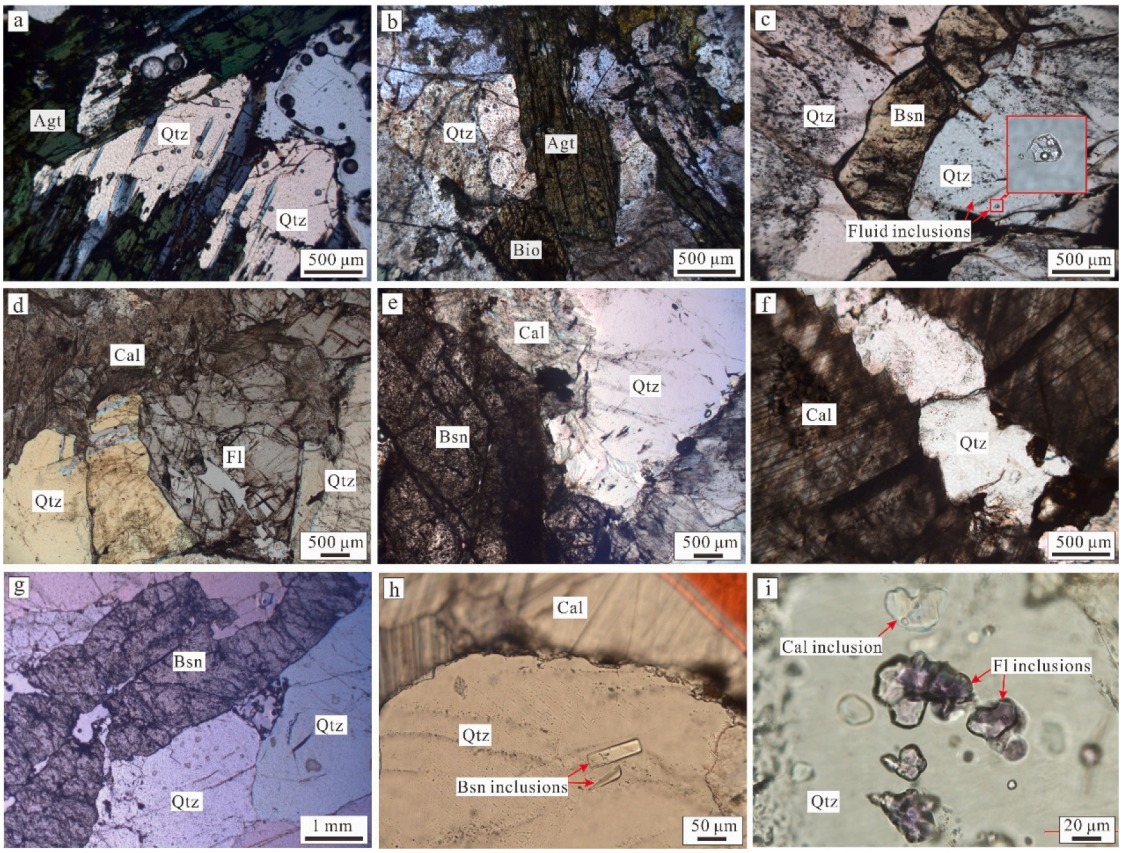

Fig. 6. Photomicrographs illustrate the occurrences of quartz in the carbonatite-related REE deposits. (a) Euhedral to subhedral quartz grains occur interstitially in the aegirine-augite in the hydrothermal veins of the Maoniuping deposit. (b) Intergrowth of quartz with aegirine-augite and biotite in the hydrothermal veins of the Maoniuping deposit. (c) Intergrowth of quartz with bastnäsite in the ores of the Maoniuping deposit. Notable that quartz contains abundant solid-bearing high salinity fluid inclusions. (d) Intergrowth of quartz with fluorite and calcite in the hydrothermal veins of the Dalucao deposit. (e) Intergrowth of quartz with bastnäsite and calcite in the ores of the Lizhuang deposit. (f) Quartz micro-veinlets crosscutting calcite in the carbonatites of the Miaoya deposit. (g) Intergrowth of quartz with bastnäsite in the ores of the Taipingzhen deposit. (h) Subhedral quartz containing euhedral bastnäsite inclusions in the ore of the Taipingzhen deposit. (i) Quartz with abundant fluorite and calcite inclusions in the Huangshuian deposit. Abbreviations: Cal = calcite, Qtz = quartz, Fl = fluorite, Agt = aegirine-augite, Bio = biotite, Bsn = bastnäsite.

zoning (Fig. 7). The CL-homogeneous texture can be observed in quartz grains from multiple mineral assemblages but the CL intensities are highly variable, even in an individual deposit. For example, CL-homogeneous quartz from the bottom unit of the Maoniuping deposit generally exhibits CL intensity higher than that from the middle and top units. Oscillatory zoning is particularly common in comb-like quartz grains of these deposits, even though it is not as conspicuous as the CL intensities for each zone which are only slightly different (Fig. 7c). In these deposits, both the homogenous and oscillatory-zoned quartz grains are overprinted by complex secondary textures related to dissolution, fracturing, overgrowth and recrystallization due to late fluid activity (Fig. 7a–b). Generally, the secondary domains have CL intensities lower than the primary ones (Fig. 7a).

4.2. Trace element compositions of quartz

The detailed trace element composition of quartz in the carbonatite-related REE deposits is provided in appendix A (Maoniuping deposit) and appendix B (other deposits), and summarized in Table 2. Concentrations of B, P, and Sn are of suspect reliability, as the quantification of these elements in quartz by the LA-ICP-MS method is severely affected by polyatomic interferences (Müller et al., 2008; Audétat et al., 2015), and thus are not used in this paper. The trace elements commonly identified in the quartz from the carbonatite-related REE deposits are Li, Na, Al, K, Ti, Ge, Fe and As, while others such as Be, Mn, Ga, Sr, Sb, and Pb are mostly below detection limits (Appendix A and B).

In general, quartz in the carbonatite-related REE deposits is characterized by low budgets of trace elements with total contents mostly less than 50 ppm (Table 2), comparable to that of the so-called high-purity quartz (Larsen et al., 2000; Müller et al., 2007, Müller et al., 2012). Aluminum is the principal trace element with concentrations ranging from 2.45 to 63.0 ppm. Titanium contents are secondary to Al, and varying from 0.68 to 12.1 ppm (Fig. 8). Alkali elements, including Li, Na and K, were detected in most analyses with average concentrations of 0.98, 2.16 and 3.45 ppm, respectively. Iron (Fe), Germanium (Ge) and Arsenic (As) have concentrations generally less than 1 ppm (Appendix A and B). Although of similar low concentrations, the trace elements in quartz exhibit slightly variations in different deposits (Fig. 8). For example, quartz from the Lizhuang deposit contains the highest concentration of trace elements and the average concentrations of Na, Al, K, and Ti are 4.3, 27.7, 9.7 and 6.7 ppm, respectively (Table 2). In contrast, quartz from the Miaoya deposit has lowest concentration of trace elements and the average concentrations of Na, Al, K and Ti are 1.2, 4.7, 0.4 and 1.1 ppm, respectively (Table 2). In all the carbonatite-related REE deposits, the content of Al in quartz is generally positively correlated with Ti, K, and Na (Fig. 9).

4.3. Spatial variation of quartz chemistry in the Maoniuping deposit

The quartz samples in hydrothermal veins of the Maoniuping deposit were systematically collected in a selected cross-section in the open pit. The locations of quartz samples, carbonatites, and orebodies are shown

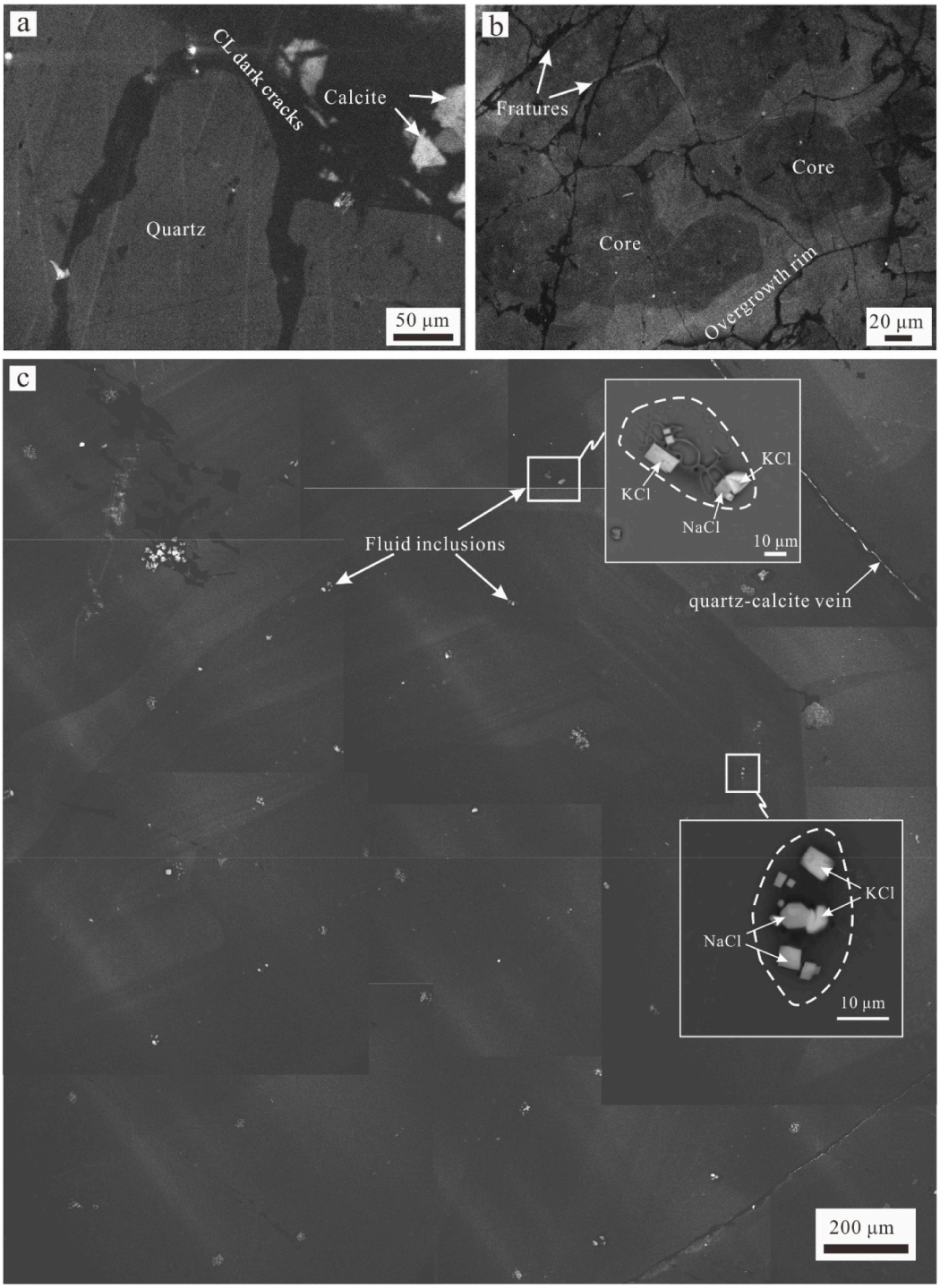

Fig. 7. CL images showing internal textures of quartz in the carboantite-related REE deposits. (a) Primary homogeneous quartz overprinted by later CL-dark quartz in the Maoniuping deposit. (b) Quartz grains in the veins comprising homogeneous cores and overgrowth rims (Huangshuian deposit). (c) Quartz from the veins exhibiting euhedral growth zones and containing abundant solid-bearing fluid inclusions (Maoniuping deposit).

in the schematic diagram of Fig. 10a and Fig. 10b. Approximately four crystals of quartz were analyzed in each sample (Appendix A), and average values of each element are used to show the spatial variation of the quartz chemistry. The spatial variations of Al, Ti, K and Na are illustrated in contour diagrams (Fig. 10c–f).

The results show that the concentrations of Al, Ti, Na, and K exhibit systematic spatial variation in the deposit. This variation is broadly correlated with the distance of samples away from the carbonatites. Generally, quartz adjacent to the carbonatites contains the highest concentrations of Al, Ti, Na, and K (Fig. 10c–f). With increase of distance from the carbonatites, the concentrations of these trace elements in quartz are gradually decreased (Fig. 10).

Table 2
Average concentrations and other statistical parameters of Li, Na, K, Al, Ti, Fe, As and total concentrations of trace elements in quartz from different carbonatite-related REE deposits.

Location		Li	Na	Al	K	Ti	Fe	Ge	As	Total
Maoniuping	Ave	1.25	2.22	17.6	3.28	3.96	0.89	0.64	0.30	30.8
	SD	1.33	2.01	11.9	2.90	1.94	0.77	0.55	0.26	17.9
	Max	7.60	15.1	62.9	18.8	12.1	4.09	3.15	1.55	98.0
	Med	0.94	1.68	14.5	2.44	4.18	0.68	0.53	0.23	26.4
	Min	0.01	0.02	3.25	0.06	0.69	0.02	0.01	0.01	5.86
	n	348	369	379	337	379	182	372	349	379
Lizhuang	Ave	0.33	4.29	27.7	9.72	6.67	0.72	0.60	0.38	50.1
	SD	0.38	1.93	13.4	5.81	1.54	0.55	0.23	0.09	21.1
	Max	1.04	8.07	57.3	22.0	10.2	1.81	1.02	0.55	95.7
	Med	0.31	3.81	26.8	8.50	6.18	0.67	0.56	0.37	47.7
	Min	0.02	0.46	5.53	0.51	4.48	0.03	0.22	0.18	12.9
	n	26	32	32	32	32	16	32	32	32
Dalucao	Ave	0.78	1.42	15.5	0.79	2.44	0.70	0.71	0.27	22.2
	SD	0.74	3.34	9.32	1.47	0.59	0.63	0.13	0.08	13.0
	Max	2.75	19.8	39.2	8.17	4.19	2.26	1.01	0.44	71.6
	Med	0.44	0.76	13.8	0.75	2.52	0.44	0.71	0.26	19.6
	Min	0.01	0.03	2.45	0.16	0.93	0.02	0.46	0.12	7.42
	n	32	32	32	21	32	13	32	32	32
Miaoya	Ave	0.03	1.24	4.68	0.43	1.10	0.89	1.57	0.12	9.42
	SD	0.01	1.24	1.60	0.50	0.28	0.56	0.25	0.11	2.78
	Max	0.05	6.20	10.4	2.10	1.63	2.48	2.00	0.45	15.8
	Med	0.02	0.67	4.10	0.63	1.10	0.72	1.56	0.08	8.68
	Min	0.02	0.08	2.90	0.21	0.18	0.33	0.93	0.04	5.70
	n	9	42	42	25	42	13	42	39	42
Taipingzhen	Ave	0.13	1.87	6.83	0.47	2.78	1.08	0.98	0.12	13.6
	SD	0.16	1.80	3.25	0.49	0.63	0.73	0.23	0.10	4.23
	Max	0.58	7.35	12.0	1.59	4.07	3.06	1.56	0.45	21.6
	Med	0.09	1.11	6.23	0.64	2.75	0.91	1.00	0.09	15.0
	Min	0.02	0.11	2.60	0.05	1.67	0.37	0.45	0.02	6.62
	n	23	35	35	23	35	14	35	33	35
Huanglongpu	Ave	0.52	2.20	17.71	5.81	2.86	1.14	0.52	0.07	30.1
	SD	0.72	2.74	8.75	4.22	0.54	0.97	0.15	0.03	14.5
	Max	2.79	10.1	32.9	0.17	4.06	3.09	0.81	0.13	54.3
	Med	0.28	1.12	17.2	5.40	2.70	0.87	0.50	0.07	29.4
	Min	0.02	0.86	3.59	13.2	2.07	0.04	0.22	0.01	8.04
	n	17	34	34	34	34	19	34	32	34
Huangshuian	Ave	0.89	1.84	14.4	2.56	3.12	1.07	0.47	0.19	23.5
	SD	0.56	1.40	6.40	1.87	0.59	0.87	0.23	0.05	8.75
	Max	1.98	5.84	28.4	7.35	3.91	3.55	0.94	0.28	41.4
	Med	0.70	1.64	13.8	1.63	3.15	0.68	0.41	0.18	24.0
	Min	0.23	0.15	4.53	0.21	1.56	0.11	0.07	0.11	9.32
	n	17	33	33	31	33	25	32	18	33

5. Discussion

5.1. Distinctive compositions of quartz in the carbonatite-related REE deposits

Our new results reveal that quartz in the carbonatite-related REE deposits is characterized by distinctly low concentrations of trace elements (Table 2). Aluminum, the dominant trace element in quartz, has concentration generally <50 ppm, whereas the concentrations of other trace elements typically do not exceed 10 ppm (Fig. 8). Such uniformly low concentration of trace elements was rarely documented in quartz from other types of magmatic-hydrothermal deposits (Fig. 11). For example, quartz from porphyry, skarn and pegmatite related deposits generally contains thousands ppm of Al, and hundreds ppm of Ti and Li (e.g., Rusk et al., 2006; Müller et al., 2010; Mao et al., 2017; Zhang et al., 2019b; Peterková and Dolejš, 2019; Rottier and Casanova, 2020; Müller et al., 2021), while that from Carlin-type Au deposits and epithermal Au-Ag deposits is commonly depleted in Ti (<10 ppm) but extremely enriched in Al (as much as 3000 ppm) and Li (hundreds of ppm) (Rusk, 2012; Maydagán et al., 2015; Li et al., 2020). Indeed, as illustrated in Fig. 11, most quartz in carbonatite-related REE deposits displays geochemistry distinguishable other magmatic-hydrothermal systems, with only a proportion of analyzes (particularly those from the Maoniuping and Lizhuang deposits) partially overlapping with those of porphyry or pegmatitic deposits.

This study further interprets that the low concentrations of trace elements in quartz from carbonatite-related REE deposits is mainly resulted from the distinctive nature of carbonatited-derived fluids. Aluminum is the dominant trace element substituting for Si^{4+} in the silicon-oxygen tetrahedra of quartz (Götze et al., 2004; Götze, 2009), which is mainly controlled by the Al content and pH values of the parental fluids (Perny et al., 1992; Rusk et al., 2008; Breiter et al., 2020). The low Al concentration of quartz in carbonatite-related REE deposits is consistent with low Al content of carbonatitic magmas/fluids, as carbonatites generally have much lower Al_2O_3 contents (commonly <1 %) compared to silicate rocks (Jones et al., 2013). For example, the carbonatites in the Maoniuping, Dalucao, Lizhuang, and Huanglongpu deposits have similarly low Al_2O_3 contents averaging at 0.11 %, 0.43 %, 1.1 % and 1.2 %, respectively (Hou et al., 2006; Xu et al., 2007). Hydrothermal fluids in carbonatite-related REE deposits should also barren in Al as they are sourced from Al-depleted carbonatitic magmas. This conclusion is supported by previous fluid inclusion investigations that show the carbonatite-related ore forming fluids generally contain extremely low Al content (Bühn and Rankin, 1999; Bühn et al., 2002; Williams-Jones and Palmer, 2002; Xie et al., 2015).

Monovalent ions including Li^+, Na^+, and K^+ are the main charge compensators for the entry of Al^{3+} into silicon-oxygen tetrahedrons (SiO_4) of quartz, via the coupled substitution Li^+ (Na^+, K^+) + Al^{3+} ↔ Si^{4+} (Dennen, 1964, 1966). This substitution is also applicable to the quartz in the carbonatite-related deposits, supported by the positive

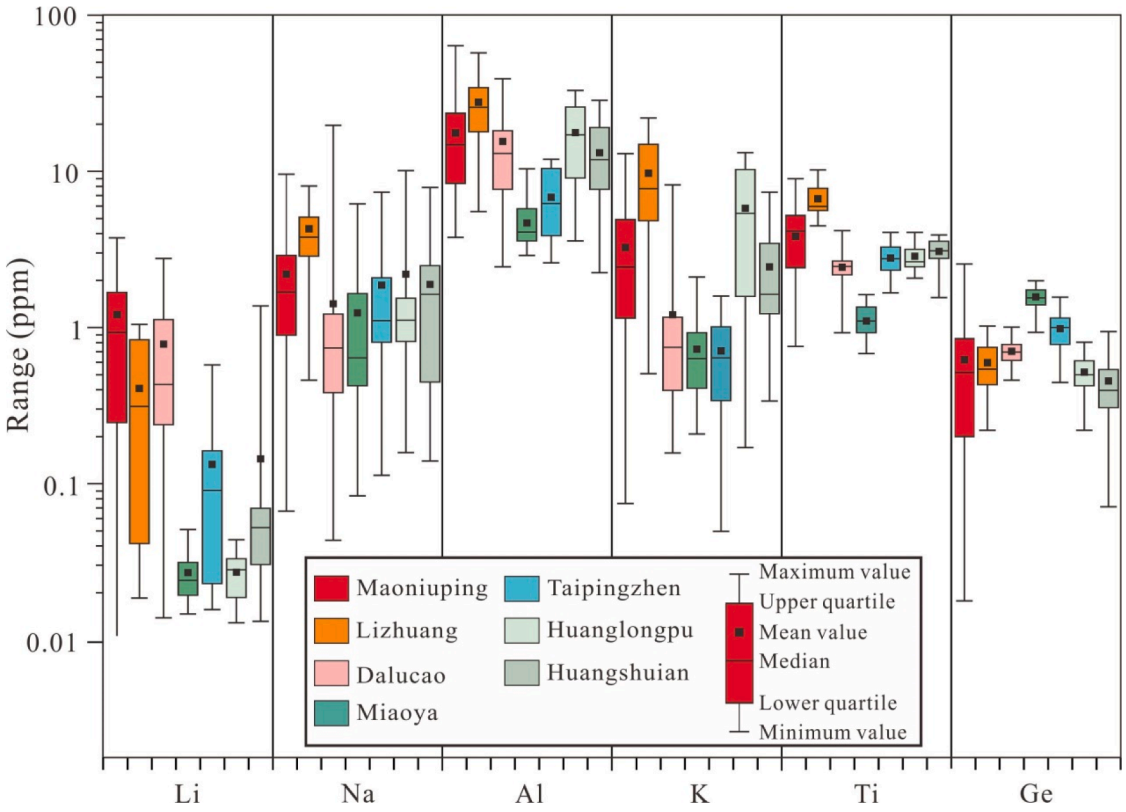

Fig. 8. Box plots showing the variation of Li, Na, Al, K, Ti and Ge in quartz from different carbonatite-related REE deposits.

correlation between the sum molar concentrations of monovalent ions (Li^+, Na^+, K^+) and Al (Fig. 12). It is important to note that the apparent excess of Al^{3+} in Fig. 12 would be related to H^+ ($H^+ + Al^{3+} \leftrightarrow Si^{4+}$) and P^{5+} ($p^{5+} + Al^{3+} \leftrightarrow 2Si^{4+}$), both of which are unable to be quantified by LA-ICP-MS (Müller et al., 2008). Therefore, although quartz in the carbonatite-related REE deposits are precipitated in hydrothermal fluids with high Na and K contents, as evidenced by the widespread alkali metasomatism (fenitization) and presence of Na-K-rich minerals such as aegirine-augite, arfvedsonite and phlogopite, incorporation of Na and K into quartz was restricted due to the low Al content of fluids.

The tetravalent ion Ti^{4+} enters the quartz lattice by substituting for Si^{4+}, and this substitution is generally controlled by magma/fluid composition, temperature and pressure (Wark and Watson, 2006; Thomas et al., 2010; Huang and Audétat, 2012). The low Ti concentration of quartz in the carbonatite-related deposits is probably constrained by the composition of magma/fluid. The carbonatites in this study generally have Ti content less than 0.1 wt% (Hou et al., 2006; Xu et al., 2007; Cangelosi et al., 2020). The Ti content of the hydrothermal fluids in these deposits is not documented but the lack of rutile and other Ti-bearing minerals indicate these fluids are Ti depleted. Another reason may cause the low Ti concentration of quartz is the low temperature. Most quartz samples in this study were collected in the orebodies with abundant bastnäsite. Previous studies have shown that fluid inclusions hosted in bastnäsite and gangue minerals (e.g., calcite, quartz, and fluorite) from the mineralization stage exhibit relatively low homogenization temperatures, generally less than 350 °C (Xie et al., 2009, 2015; Wu et al., 2011; Shu and Liu, 2019; Zheng and Liu, 2019; Tang et al., 2021; Zhang et al., 2022). The TitaniQ thermobarometer show that quartz formed at this temperature has extremely low concentration of Ti (<5 ppm) even Ti is saturated in the fluid (Wark and Watson, 2006; Huang and Audétat, 2012).

5.2. Variation of quartz chemistry among different deposits

Although of similarly low contents of trace elements, it can be observed in Fig. 8 and Table 2 that quartz grains from different carbonatite-related deposits do have different geochemical compositions. Our results show that quartz grains from the Mianning-Dechang REE belt (Maoniuping, Lizhuang, and Dalucao deposits) have Al, K, and Na contents higher than those from the Qinling belt (Miaoya, Taipingzhen, Huangshuian and Huanglongpu deposits) (Table 2). Such a chemical variation could be interpreted to be related to variable intensities of fenitization. The reason is that during the fenitization, a portion of Al is released into the fluid by dissolving Al-bearing minerals (e.g., feldspar) in the wall rocks (Morogan, 1989; Drppel et al., 2005; Elliott et al., 2018). Therefore, the high Al in the quartz grains of the Mianning-Dechang belt could be ascribed to the much more intensive and widespread fenitization (Hou et al., 2009; Xie et al., 2015; Liu et al., 2019) relative to those of the Qinling REE belt (Xu et al., 2014; Ying et al., 2017; Bai et al., 2019; Zhang et al., 2019a). The high Al contents in turn promote the incorporation of Na and K into the lattice of quartz as the two elements are charge compensators for the entry of Al into silicon-oxygen tetrahedrons.

5.3. Fluid evolution-controlled spatial variation of quartz chemistry at the Maoniuping deposit

Detailed trace elemental analyses of quartz from a cross-section in the Maoniuping deposit reveal a systematic, spatial variation of quartz composition, which corresponds roughly to the distance of samples away from the causative carbonatites (Fig. 10). This spatial variation is related to the variation of physio-chemical conditions during the evolution of carbonatite-derived ore-forming fluids.

The concentration of Al in quartz is gradually decreased with the increase of distance from carbonatites (Fig. 10c). The spatial variation of Al in the quartz can be explained by the systematic change of Al contents

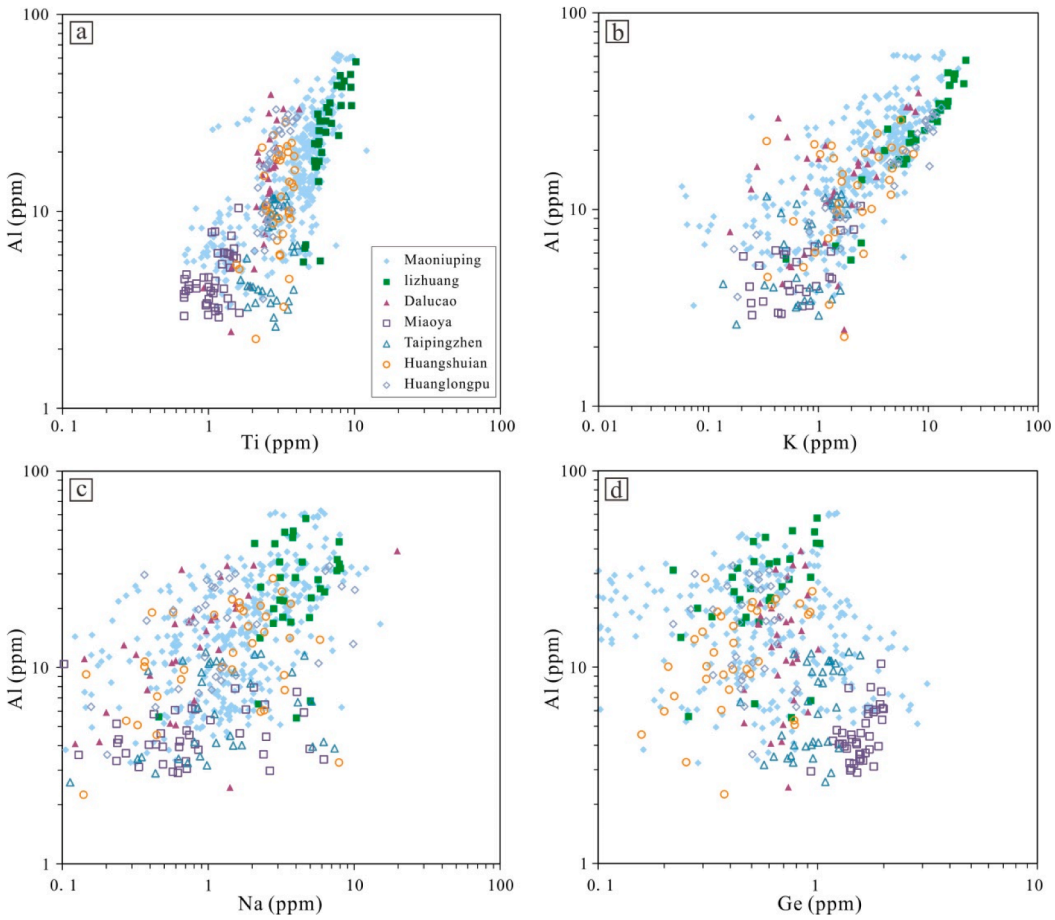

Fig. 9. Correlation plots of Al vsTi (a), Al vsK (b), Al vsNa (c) and Al vsGe (d) for quartz in the carbonatite-related REE deposits.

in the fluids. In the case of Maoniuping, fenitization of wall rocks and crystallization of Al-rich minerals are two dominant mechanisms leading the variation of Al in the fluid. At the very beginning, the carbonatitic melt-exsolved fluids with relatively high temperatures will interact with the wall rocks, producing intensive fenitization. During this process, Al is able to be leached into the fluids through dissolving feldspar in the wall rocks (Morogan, 1989; Elliott et al., 2018). As the fluid migrates outwards, the intensity of fenitization decreased systemically due to consumption of alkaline ions and drop of temperatures (Fig. 10a), which would gradually reduce contributions of Al from wall rocks. Moreover, the precipitation of some Al-bearing minerals, such as phlogopite, K-feldspar and biotite during fluid evolution is able to consume Al, consequently drop the Al contents in the fluids. This interpretation is consistent well with the spatial and systematic variation of Al in quartz, i. e., gradually decreased with increase of distance from the causative carbonatites (Fig. 10c). On the other hand, the spatial variations of Na and K correlate well with that of Al (Fig. 10 e–f), which could be simply explained by the fact that these monovalent ions have to counterbalance with Al to incorporate the lattice of quartz.

The concentration of Ti has similar spatial variation to Al, Na and K, that is gradually decreased with the increase of distances from carbonatites (Fig. 10d). Such variation is interpreted to be caused by the decrease of temperature during the migration of ore forming fluids. This conclusion is supported by recent investigation of fluid inclusion that reveals the temperatures of ore-forming fluids are gradually decreased from bottom (~480 °C) to top (260 to 350 °C) units in the Maoniuping deposit (Zheng and Liu, 2019).

5.4. General implications

In addition to carbonatites, REE mineralization also associates with other magmatic-hydrothermal systems, e.g., alkaline (syenite), pegmatite (Dostal 2016; London 2016). Therefore, defining affinity of REE mineralization is crucial for regional exploration, but is often challenging particularly for those deposits in which the whole mineralization system is partially outcropped and/or partially modified due to extensive weathering. Our results show that quartz in the carbonatite-related REE deposits contain extremely low concentrations of trace elements including Al, Li, Na, K and Ti, clearly different from quartz associated with other magmatic-hydrothermal systems (Fig. 11). We suggest that quartz chemistry may be a useful tool for understanding affinity of undefined hydrothermal REE systems that do not show clear spatial association with potential causative intrusions, such as the the Karrat Isfjord REE deposit in the Central West Greenland (Mott et al., 2013), and the Hoidas Lake REE deposit in Northern Saskatchewan, Canada (Pandur et al., 2016).

Carbonatites are the source of ore-forming fluids and thus are the center and even hosts of REE mineralization in many carbonatite-related REE deposits (Chakhmouradian and Zaitsev, 2012; Verplanck et al., 2016; Simandl and Paradis, 2018). Therefore, precisely identifying the concealed carbonatites is critical for exploration of such kind of REE deposits. Our study reveals that quartz chemistry exhibits a systematic, spatial variation that correlates roughly with the distance of samples away from the causative carbonatites, as documented in the Maoniuping deposit (Fig. 10). We thus propose that the trace element chemistry of quartz can be also used as an important vector to the causative carbonatites.

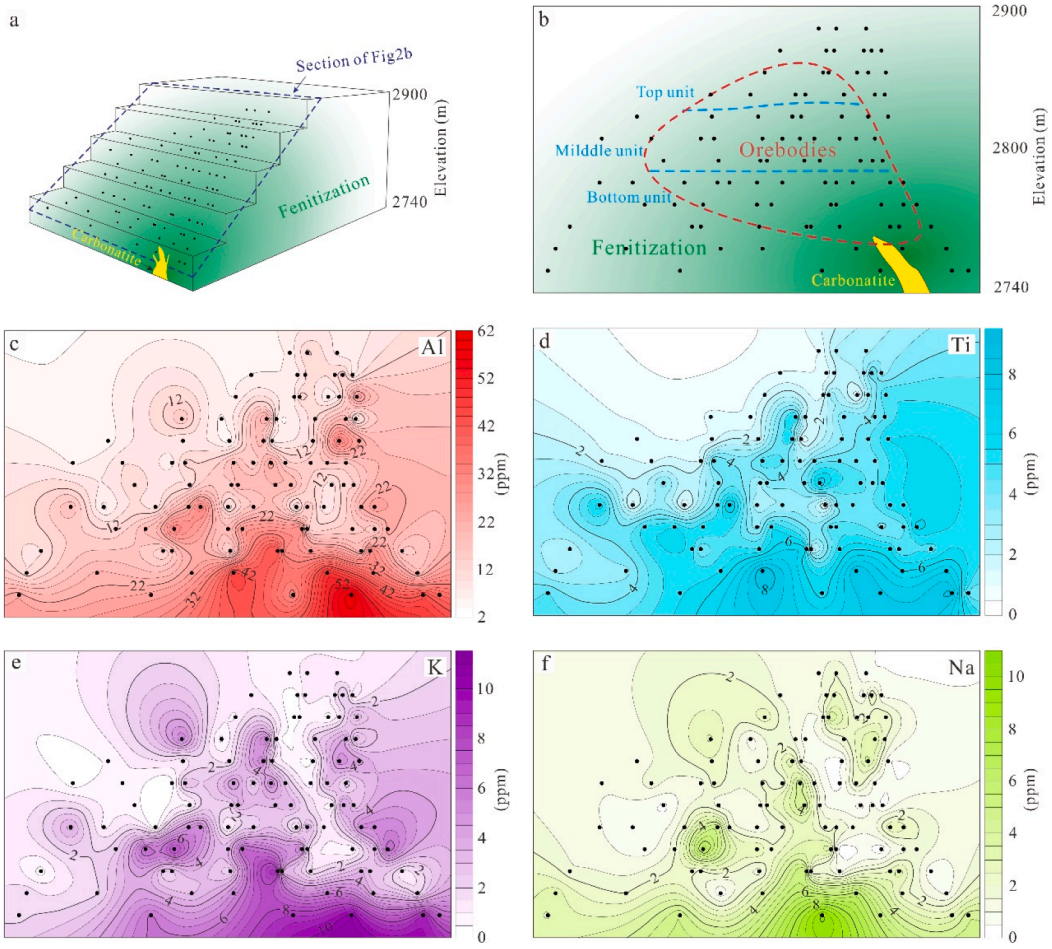

Fig. 10. (a) A 3D cartoon of the benches in the Maoniuping open mine, showing direction of the cross-section in Fig. 2b, as well as sample locations and fenitization intensity. (b) A plan view of the cross-section, illustrating the spatial relationships among the sample locations, carbonatites, orebodies and fenitization. (c-f) Isopleth diagrams showing the spatial variations of Al (c), Ti (d), K (e), and Na (f) in quartz of the plan view (b) of the cross-section.

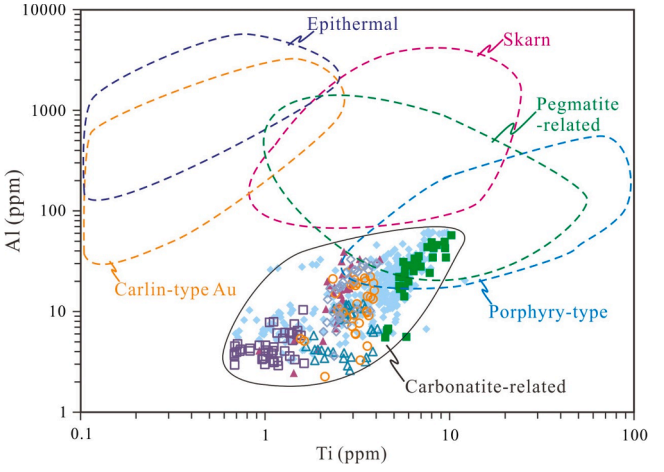

Fig. 11. Discrimination diagrams of Al-Ti for quartz in the the carbonatite-related REE deposits. The diagram is adapted from Rusk (2012) and the field for porphyry-type deposits is drawn through the data from Landtwing and Pettke (2005), Allan and Yardley (2007), Maydagán et al. (2015), Mao et al. (2017) and Rottier and Casanova (2020), that for skarn deposits is from Zhang et al. (2019b), that for pegmatite related deposits is from Peterková and Dolejš (2019) and Müller et al. (2021), that for epithermal deposits is from Rusk et al. (2011) and Tanner et al. (2013), and that for Carlin-type Au deposits is from Li et al. (2020) and Yan et al. (2020).

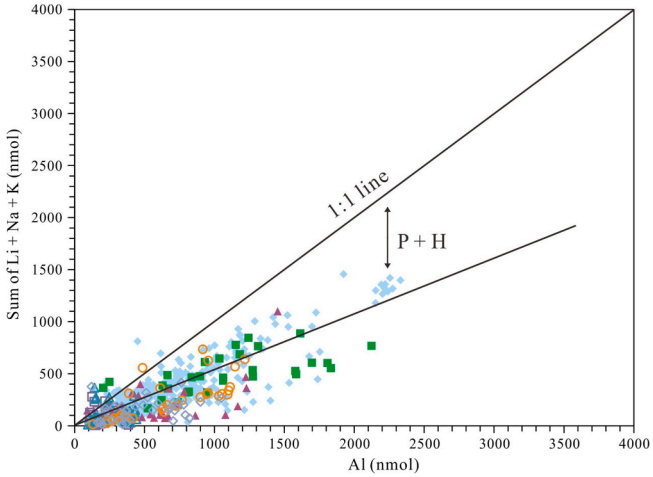

Fig. 12. Correlation plot of total molar concentrations (nmol) of monovalent cations (Li, Na, K) vs Al. Note that Li + Na + K is broadly positively correlated with Al, indicative of a substitution mechanism of $(Li^{+}+Na^{+}+K^{+}) + Al^{3+} \leftrightarrow Si^{4+}$. The derivation from the 1:1 line is possibly ascribed to the lack of H^{+} and P^{5+} data which are not available in this study.

Declaration of Competing Interest

The authors declare that they have no known competing financial interests or personal relationships that could have appeared to influence the work reported in this paper.

Data availability

Data will be made available on request.

Acknowledgements

This study is supported by the National Natural Science Foundation of China (42121003, 42103065, 41822303). Additional support was provided by Key Research Program of Frontier Sciences, CAS (QYZDB-SSW-DQC008). We appreciate Yong Fan from 109 Team of Geology, Sichuan Bureau of Geology and Mineral Resources and Hua-Kai Chen and Jing-Hui Li from Henan Nuclear Geological Bureau for the field assistance. We also thank Shao-Hua Dong and Jun-Jie Han from the State Key Laboratory of Ore Deposit Geochemistry, Institute of Geochemistry, Chinese Academy of Sciences, for the help during BSE and LA-ICP-MS analyses. We are grateful to Hua-Yong Chen for editorial handling, and Loïs Monnier and an anonymous reviewer for their detailed and insightful suggestions.

Appendix A. Supplementary data

Supplementary data to this article can be found online at https://doi.org/10.1016/j.oregeorev.2022.105068.

References

Allan M, M, Yardley W. D, B, 2007. Tracking meteoric infiltration into a magmatic-hydrothermal system: A cathodoluminescence, oxygen isotope and trace element study of quartz from Mt. Leyshon, Australia. Chem. Geol. 240 (3–4), 343–360.

Audétat, A., Garbe-Schönberg, D., Kronz, A., Pettke, T., Rusk, B., Donovan, J.J., Lowers, H.A., 2015. Characterisation of a natural quartz crystal as a reference material for microanalytical determination of Ti, Al, Li, Fe, Mn, Ga and Ge. Geostand. Geoanal. Res. 39, 171–184.

Bai, T., Chen, W., Jiang, S.Y., 2019. Evolution of the carbonatite Mo-HREE deposits in the Lesser Qinling Orogen: Insights from in situ geochemical investigation of calcite and sulfate. Ore Geol. Rev. 113, 103069.

Breiter, K., Ackerman, L., Svojtka, M., Müller, A., 2013. Behavior of trace elements in quartz from plutons of different geochemical signature: A case study from the Bohemian Massif, Czech Republic. Lithos 175, 54–67.

Breiter, K., Ďurišová, J., Dosbaba, M., 2017. Quartz chemistry–A step to understanding magmatic-hydrothermal processes in ore-bearing granites: Cínovec/Zinnwald Sn-W-Li deposit. Central Europe. Ore Geol. Rev. 90, 25–35.

Breiter, K., Ďurišová, J., Dosbaba, M., 2020. Chemical signature of quartz from S-and A-type rare-metal granites–A summary. Ore Geol. Rev. 125, 103674.

Bühn, B., Rankin, A.H., 1999. Composition of natural, volatile-rich Na-Ca-REE-Sr carbonatitic fluids trapped in the fluid inclusions. Geochim. Cosmochim. Acta 63, 3781–3797.

Bühn, B., Rankin, A.H., Schneider, J., Dulski, P., 2002. The nature of orthomagmatic, carbonatitic fluids precipitating REE, Sr-rich fluorite. fluid-inclusion evidence from the Okorusu fluorite deposit. Namibia. Chem. Geol. 186, 75–98.

Cangelosi, D., Smith, M., Banks, D., Yardley, B., 2020. The role of sulfate-rich fluids in Heavy Rare Earth enrichment at the Dashigou carbonatite deposit, Huanglongpu. China. Mineral. Mag. 84, 65–80.

Cao, J., Ye, H.S., Li, H.Y., Li, Z.Y., Zhang, X.K., He, W., Li, C., 2014. Geological characteristics and molybdenite Re-Os isotopic dating of Huangshuian carbonatite vein-type Mo (Pb) deposit in Songxian County, Henan Province. Mineral Deposits 33, 53–69 in Chinese with English abstract.

Chakhmouradian, A.R., Zaitsev, A.N., 2012. Rare Earth Mineralization in Igneous Rocks: Sources and Processes. Elements 8, 347–353.

Cong, B.L., 1988. Formation and evolution of the Panxi Paleo-rift. Science Press, Beijing (in Chinese with English abstract).

Dennen, W.H., 1964. Impurities in quartz. Geol. Soc. Am. Bull. 75, 241–246.

Dennen, W.H., 1966. Stoichiometric substitution in natural quartz. Geochim. Cosmochim. Acta 30, 1235–1241.

Dostal, J., 2016. Rare metal deposits associated with alkaline/peralkaline igneous rocks. in Verplanck P. L., and Hitzman M. W., eds., Rare earth and critical elements in ore deposits. Society of Economic Geologists 18, 33-54.

Drppel, K., Hoefs, J., Okrusch, M., 2005. Fenitizing Processes Induced by Ferrocarbonatite Magmatism at Swartbooisdrif, NW Namibia. J. Petrol. 46, 377–406.

Elliott, H.A.L., Wall, F., Chakhmouradian, A.R., Siegfried, P.R., Dahlgren, S., Weatherley, S., Finch, A.A., Marks, M.A.W., Dowman, E., Deady, E., 2018. Fenites associated with carbonatite complexes: A review. Ore Geol. Rev. 93, 38–59.

Gao, C., Kang, Q.Q., Jiang, H.J., Zheng, H., Li, P., Zhang, X.M., Li, L., Dong, Q.Q., Ye, X. C., Hu, X.J., 2017. A unique uranium polymetallic deposit discovered in the Qinling orogenic belt: The Huayangchuan super-large U-Nb-Pb-REE deposit associated with pegmatites and carbonatites. Geochimica. 46, 446–455 in Chinese with English abstract.

Götze, J., 2009. Chemistry, textures and physical properties of quartz – geological interpretation and technical application. Mineral. Mag. 73, 645–671.

Götze, J., Plötze, M., Graupner, T., Hallbauer, D.K., Bray, C.J., 2004. Trace element incorporation into quartz: A combined study by ICP-MS, electron spin resonance, cathodoluminescence, capillary ion analysis, and gas chromatography 1. Geochim. Cosmochim. Acta 68, 3741–3759.

Hou, Z., Tian, S., Yuan, Z., Xie, Y., Yin, S., Yi, L., Fei, H., Yang, Z., 2006. The Himalayan collision zone carbonatites in western Sichuan, SW China: Petrogenesis, mantle source and tectonic implication. Earth Planet. Sci. Lett. 244, 234–250.

Hou, Z., Tian, S., Xie, Y., Yang, Z., Yuan, Z., Yin, S., Yi, L., Fei, H., Zou, T., Bai, G., 2009. The Himalayan Mianning–Dechang REE belt associated with carbonatite–alkaline complexes, eastern Indo-Asian collision zone. SW China. Ore Geol. Rev. 36, 65–89.

Huang, R., Audétat, A., 2012. The titanium-in-quartz (TitaniQ) thermobarometer: A critical examination and re-calibration. Geochim. Cosmochim. Acta 84, 75–89.

Jones, A.P., Genge, M.J., Carmody, L., 2013. Carbonate melts and carbonatites. Rev. Mineral. Geochem. 75, 289–322.

Kynicky, J., Smith, M.P., Xu, C., 2012. Diversity of Rare Earth Deposits: The Key Example of China. Elements. 8, 361–367.

Lan, T.G., Hu, R.Z., Bi, X.W., Mao, G.J., Wen, B.J., Liu, L., Chen, Y.H., 2017. Metasomatized asthenospheric mantle contributing to the generation of Cu-Mo deposits within an intracontinental setting: A case study of the~128 MaWangjiazhuang Cu-Mo deposit, eastern North China Craton. J. Asian Earth Sci. 160, 460–489.

Landtwing, M.R., Pettke, T., 2005. Relationships between SEM-cathodoluminescence response and trace-element composition of hydrothermal vein quartz. Am. Miner. 90, 122–131.

Larsen, R.B., Polvé, M., Juve, G., 2000. Granite pegmatite quartz from Evje-Iveland: trace element chemistry and implications for the formation of high-purity quartz. Norges Geologiske Undersøkelse Bull. 436, 57–65.

Launay, G., Sizaret, S., Lach, P., Melleton, J., Gloaguen, E., Poujol, M., 2021. Genetic relationship between greisenization and Sn-W mineralizations in vein and greisen deposits: Insights from the Panasqueira deposit (Portugal). Bullet. Société Géologique de France 192, 1–26.

Li, J.H., Chen, H.K., Zhang, H.W., Zhang, Y.H., Zhang, T.L., Wen, G.D., Zhang, P.P., 2017. Mineralization characteristics and ore genesis of the light rare earth deposit in Taiping Town, western Henan. Geology in China 44, 288–300 in Chinese with English abstract.

Li, J.W., Hu, R.Z., Xiao, J.F., Zhuo, Y.Z., Yan, J., Oyebamiji, A., 2020. Genesis of gold antimony deposits in the Youjiang metallogenic province, SW China: Evidence from in situ oxygen isotopic and trace element compositions of quartz. Ore Geol. Rev. 116, 103257.

Liu, Y., Chakhmouradian, A.R., Hou, Z., Song, W., Kynicky, J., 2019. Development of REE mineralization in the giant Maoniuping deposit (Sichuan, China): insights from mineralogy, fluid inclusions, and trace-element geochemistry. Miner. Depos. 54, 701–718.

Liu, Y.S., Hu, Z.C., Gao, S., Günther, D., Xu, J., Gao, C., Chen, H., 2008. In situ analysis of major and trace elements of anhydrous minerals by LA-ICP-MS without applying an internal standard. Chem. Geol. 257, 34–43.

London, D., 2016. Rare-element granitic pegmatites. in Verplanck P. L., and Hitzman M. W., eds., Rare earth and critical elements in ore deposits. Society of Economic Geologists 18, 165-193.

Luo, Y.N., Yu, R.L., Hou, L.W., Lai, S.M., Fu, D.M., Chen, M.X., Fu, X.Y., Rao, R.B., Zhou, S.S., 1998. Longmenshan-Jinpingshan Intracontinental Orogenic Belt. Sichuan Science and Technology Publishing House, Chengdu.

Mao, W., Rusk, B., Yang, F., Zhang, M., 2017. Physical and chemical evolution of the dabaoshan porphyry Mo deposit, South China: Insights from fluid inclusions, cathodoluminescence, and trace elements in quartz. Econ. Geol. 112, 889–918.

Maydagán, L., Franchini, M., Rusk, B., Lentz, D.R., Mcfarlane, C., Impiccini, A., Rios, F.J., Rey, R., 2015. Porphyry to epithermal transition in the altar Cu-(Au-Mo) Deposit, Argentina, studied by cathodoluminescence, LA-ICP-MS, and fluid inclusion analysis. Econ. Geol. 110, 889–923.

Monnier, L., Lach, P., Salvi, S., Melleton, J., Bailly, L., Béziat, D., Monnier, Y., Gouy, S., 2018. Quartz trace-element composition by LA-ICP-MS as proxy for granite differentiation, hydrothermal episodes, and related mineralization: The Beauvoir Granite (Echassières district), France. Lithos 320–321, 355–377.

Monnier, L., Salvi, S., Pochon, A., Melleton, J., Béziat, D., Lach, P., Bailly, L., 2021. Antimony in quartz as a vector to mineralization: A statistical approach from five Variscan Sb occurrences (France). J. Geochem. Explor. 221, 106705.

Morogan, V, 1989. Mass transfer and REE mobility during fenitization at Alnö, Sweden. Contrib. Mineral. Petrol. 103, 25–34.

Mott, A.V., Bird, D.K., Grove, M., Rose, N., Bernstein, S., Mackay, H., Krebs, J., 2013. Karrat, Isfjord: A newly discovered Paleoproterozoic carbonatite-sourced REE deposit, Central West Greenland. Econ. Geol. 108, 1471–1488.

Müller, A., Wanvik, J.E., Ihlen, P.M., 2012. Petrological and chemical characterisation of high-purity quartz deposits with examples from norway. in Gotze, J., and Mockel, R., eds., Quartz: Deposits, mineralogy and analytics, 1st ed. Springer Geology, 71–118.

Müller, A., Ihlen, P.M., Wanvik, J.E., Flem, B., 2007. High-purity quartz mineralisation in kyanite quartzites. Norway. Miner. Depos. 42, 523–535.

Müller, A., Wiedenbeck, M., Flem, B., Schiellerup, H., 2008. Refinement of phosphorus determination in quartz by LA-ICP-MS through defining new reference material values. Geostand. Geoanal. Res. 32, 361–376.
Müller, A., Herrington, R., Armstrong, R., Seltmann, R., Kirwin, D.J., Stenina, N.G., Kronz, A., 2010. Trace elements and cathodoluminescence of quartz in stockwork veins of Mongolian porphyry-style deposits. Miner. Depos. 45, 707–727.
Müller, A., Keyser, W., Simmons, W.B., Webber, K., Wise, M., Beurlen, H., Garate-Olave, I., Roda-Robles, E., Galliski, M.A., 2021. Quartz chemistry of granitic pegmatites: Implications for classification, genesis and exploration. Chem. Geol. 584, 120507.
Pandur, K., Ansdell, K.M., Kontak, D.J., Halpin, K.M., Creighton, S., 2016. Petrographic and mineral chemical characteristics of the Hoidas Lake deposit, Northern Saskatchewan, Canada: Constraints on the origin of a distal magmatic-hydrothermal REE system. Econ. Geol. 111, 667–694.
Pearce, N.J.G., Perkins, W.T., Westgate, J.A., Gorton, M.P., Jackson, S.E., Nael, C.R., Chenery, S.P., 1997. Compilation of new and published major trace element data for NIST SRM 610 and NIST SRM 612 glass reference materials. Geostandards Newsletter 21, 115–144.
Perny, B., Eberhardt, P., Ramseyer, K., Mullis, J., Pankrath, R., 1992. Microdistribution of Al, Li, and Na in α quartz: Possible causes and correlation with short-lived cathodoluminescence. Am. Mineral. 77, 534–544.
Peterková, T., Dolejš, D., 2019. Magmatic-hydrothermal transition of Mo-W-mineralized granite-pegmatite-greisen system recorded by trace elements in quartz: Krupka district, Eastern Krušné hory/Erzgebirge. Chem. Geol. 523, 179–202.
Qian, D.D., Li, J.Q., 1996. The discovering History of Chinese Deposits: Hubei Volume: Geological Publishing House. Beijing (in Chinese).
Qu, K., Fan, G., Li, G., Sima, X., Chen, H., Liu, X., Ge, X., Yu, A., 2019a. Mineralogy of törnebohmite-(Ce) discovered for the first time in China. Acta Mineral. Sin. 39, 133–142 in Chinese with English abstract.
Qu, K., Sima, X., Li, G., Fan, G., Li, T., Guo, H., Yin, Q., Li, J., 2019b. Mineralogical study of the fluocerite-(La) found firstly in China. Bull. Mineral. Petrol. Geochem. 38, 764–772 in Chinese with English abstract.
Qu, K., Sima, X., Fan, G., Li, G., Shen, G., Chen, H., Liu, X., Yin, Q., Li, T., Wang, Y., 2020. Taipingite-(Ce), (Ce73+, Ca2)9Mg(SiO4)3[SiO3(OH)]4F3), a new mineral from the Taipingzhen REE deposit, North Qinling Orogen, central China. Geosci. Front. 11, 2339–2346.
Rankin, A.H., 2005. Carbonatite-associated rare metal deposits: composition and evolution of ore-forming fluids-the fluid inclusion evidence. Geol. Assoc. Canada, Short Course Notes 17, 299–314.
Rottier, B., Casanova, V., 2020. Trace element composition of quartz from porphyry systems: a tracer of the mineralizing fluid evolution. Miner. Depos. 56, 843–862.
Rusk, B., 2012. Cathodoluminescent textures and trace elements in hydrothermal quartz. In: Gotze, J., Mockel, R. (Eds.), Quartz: Deposits, Mineralogy and Analytics, 1st ed. Springer Geology, pp. 307–329.
Rusk, B., Koenig, A., Lowers, H., 2011. Visualizing trace element distribution in quartz using cathodoluminescence, electron microprobe, and laser ablation-inductively coupled plasma-mass spectrometry. Am. Miner. 96, 703–708.
Rusk, B.G., Reed, M.H., Dilles, J.H., Kent, A.J.R., 2006. Intensity of quartz cathodoluminescence and trace-element content in quartz from the porphyry copper deposit at Butte, Montana. Am. Miner. 91, 1300–1312.
Rusk, B.G., Lowers, H.A., Reed, M.H., 2008. Trace elements in hydrothermal quartz: Relationships to cathodoluminescent textures and insights into vein formation. Geology 36, 547–550.
Shu, X., Liu, Y., 2019. Fluid inclusion constraints on the hydrothermal evolution of the Dalucao carbonatite-related REE deposit, Sichuan Province, China. Ore Geol. Rev. 107, 41–57.
Simandl, G.J., Paradis, S., 2018. Carbonatites: related ore deposits, resources, footprint, and exploration methods. Appl. Earth Sci. 4, 123–152.
Smith, M., Kynicky, J., Xu, C., Song, W., Spratt, J., Jeffries, T., Brtnicky, M., Kopriva, A., Cangelosi, D., 2018. The origin of secondary heavy rare earth element enrichment in carbonatites: Constraints from the volution of the Huanglongpu district, China. Lithos 308–309, 65–82.
Song, W., Xu, C., Qi, L., Zhou, L., Wang, L., Kynicky, J., 2015. Genesis of Si-rich carbonatites in Huanglongpu Mo deposit, Lesser Qinling orogen, China and significance for Mo mineralization. Ore Geol. Rev. 64, 756–765.
Song, W., Xu, C., Smith, M.P., Kynicky, J., Huang, K., Wei, C., Zhou, L., Shu, Q., 2016. Origin of unusual HREE-Mo-rich carbonatites in the Qinling orogen. China. Sci. Rep. 6, 373–377.
Tang, L., Wagner, T., Fusswinkel, T., Zhang, S., Xu, B., Jia, L., Hu, X., 2021. Magmatic-hydrothermal evolution of an unusual Mo-rich carbonatite: a case study using LA-ICP-MS fluid inclusion microanalysis and He-Ar isotopes from the Huangshui'an deposit, Qinling, China. Miner. Depos. 56, 1133–1150.
Tanner, D., Henley, R.W., Mavrogenes, J.A., Holden, P., 2013. Combining in situ isotopic, trace element and textural analyses of quartz from four magmatic-hydrothermal ore deposits. Contrib. Mineral. Petrol. 166, 1119–1142.
Thomas, J.B., Watson, E.B., Spear, F.S., Shemella, P.T., Nayak, S.K., Lanzirotti, A., 2010. TitaniQ under pressure: the effect of pressure and temperature on the solubility of Ti in quartz. Contrib. Mineral. Petrol. 160, 743–759.
Verplanck, P.L., Mariano, A.N., Mariano, A.J., 2016. Rare earth element ore geology of carbonatites. in: Verplanck P L and Hitzman M W, eds. Rare earth and critical elements in ore deposits. Reviews in Econ. Geol. 18, 5-32.
Walter, B.F., Giebel, R.J., Steele-Macinnis, M., Marks, M.A.W., Kolb, J., Markl, G., 2021. Fluid associated with carbonatitic magmatism: A critical review and implications for carbonatite magma ascent. Earth-Sci. Rev. 215, 103509.
Wark, D.A., Watson, E.B., 2006. TitaniQ: a titanium-in-quartz geothermometer. Contrib. Mineral. Petrol. 152, 743–754.
Williams-Jones, A.E., Palmer, D.A.S., 2002. The evolution of aqueous-carbonic fluids in the Amba Dongar carbonatite, India: implications for fenitisation. Chem. Geol. 185, 283–301.
Wu, M., Xu, C., Wang, J., Song, W., 2011. A preliminary study on genesis of REE deposit in Miaoya. Acta Mineral. Sin. 31, 478–484 in Chinese with English abstract.
Xie, Y.L., Hou, Z.Q., Goldfarb, R.J., Guo, X., Wang, L., 2016. Rare earth element deposits in China. in Verplanck, P.L., and Hitzman, M.W., eds., Rare earth and critical elements in ore deposits. Society of Economic Geologists 18, 115-136.
Xie, Y.L., Hou, Z.Q., Yin, S.P., Dominy, S.C., Xu, J.H., Tian, S.H., Xu, W.Y., 2009. Continuous carbonatitic melt-fluid evolution of a REE mineralization system: Evidence from inclusions in the Maoniuping REE deposit, Western Sichuan. China. Ore Geol. Rev. 36, 90–105.
Xie, Y.L., Li, Y.X., Hou, Z.Q., Cooke, D.R., Danyushevsky, L., Dominy, S.C., Yin, S.P., 2015. A model for carbonatite hosted REE mineralisation — the Mianning–Dechang REE belt, Western Sichuan Province. China. Ore Geol. Rev. 70, 595–612.
Xu, C., Campbell, I.H., Allen, C.M., Huang, Z.L., Qi, L., Zhang, H., Zhang, G.S., 2007. Flat rare earth element patterns as an indicator of cumulate processes in the Lesser Qinling carbonatites, China. Lithos 95, 267–278.
Xu, C., Kynicky, J., Chakhmouradian, A.R., Qi, L., Song, W., 2010. A unique Mo deposit associated with carbonatites in the Qinling orogenic belt, central China. Lithos 118, 50–60.
Xu, C., Chakhmouradian, A.R., Taylor, R.N., Kynicky, J., Li, W., Song, W., Fletcher, I.R., 2014. Origin of carbonatites in the South Qinling orogen: Implications for crustal recycling and timing of collision between the South and North China Blocks. Geochim. Cosmochim. Acta 143, 189–206.
Yan, J., Mavrogenes, J.A., Liu, S., Coulson, I.M., 2020. Fluid properties and origins of the Lannigou Carlin-type gold deposit, SW China: Evidence from SHRIMP oxygen isotopes and LA-ICP-MS trace element compositions of hydrothermal quartz. J. Geochem. Explor. 215, 106546.
Ying, Y., Chen, W., Lu, J., Jiang, S.Y., Yang, Y., Ying, Y., Chen, W., Lu, J., Jiang, S.Y., Yang, Y., 2017. In situ U-Th-Pb ages of the Miaoya carbonatite complex in the South Qinling orogenic belt, central China. Lithos 290–291, 159–171.
Yuan, Z.X., Shi, Z.M., Bai, G., Wu, C.Y., Chi, R.A., Li, X.Y., 1995. The Maoniuping Rare Earth Ore Deposit. Seismological Press, Beijing, Mianning County, Sichuan Province.
Zhang, W., Chen, T.W., Gao, J.F., Chen, H.K., Li, J.H., 2019a. Two episodes of REE mineralization in the Qinling Orogenic Belt, Central China: In-situ U-Th-Pb dating of bastnäsite and monazite. Miner. Depos. 54, 1265–1280.
Zhang, Y., Chen, J.M., Tian, J., Pan, J., Sun, S.Q., Zhang, L.J., Zhang, S.T., Chu, G.B., Zhao, Y.J., Lai, C., 2019b. Texture and trace element geochemistry of quartz in skarn system: Perspective from Jiguanzui Cu-Au skarn deposit. Eastern China. Ore Geol. Rev. 109, 535–544.
Zhang, W., Chen, H.K., Li, J.H., Gao, J.F., Chen, T.W., Zhang, X.C., Tang, Y.W., 2021. Composition of ore-forming fluids in the Huangshuian carbonatite-related Mo-(REE) deposit: Insights from LA-ICP-MS analyses of fluid inclusions. Ore Geol. Rev. 136, 104284.
Zhang, W., Chen, T.W., Mernagh, T.P., Zhou, L., 2022. Quantifying the nature of ore-forming fluids in the Dalucao carbonatite-related REE deposit, Southwest China: implication for the transport and deposition of REEs. Miner. Depos. 57, 935–953.
Zheng, H., Chen, H., Li, D., Wu, C., Lai, C.K., 2020. Timing of carbonatite-hosted U-polymetallic mineralization in the supergiant Huayangchuan deposit, Qinling Orogen: Constraints from titanite U-Pb and molybdenite Re–Os dating. Geosci Front. 11, 1581–1592.
Zheng, X., Liu, Y., 2019. Mechanisms of element precipitation in carbonatite-related rare-earth element deposits: Evidence from fluid inclusions in the Maoniuping deposit, Sichuan Province, south western China. Ore Geol. Rev. 107, 218–238.